Synthesis and Comparative Reactivity and Electronic Structural Features of [MFe₃S₄]$^{z+}$ Cubane-Type Clusters (M = Fe, Co, Ni)

Jian Zhou,[†] Michael J. Scott,[†] Zhengguo Hu,[§] Gang Peng,[†] E. Münck,[*,§] and R. H. Holm[*,†]

Contribution from the Departments of Chemistry, Harvard University, Cambridge, Massachusetts 02138, and Carnegie Mellon University, Pittsburgh, Pennsylvania 15213. Received July 2, 1992. Revised Manuscript Received August 27, 1992

Abstract: The heterometal cubane-type clusters [CoFe₃S₄(Smes)₄]$^{2-}$ (**7**, 80%) and [NiFe₃S₄(PPh₃)(Smes)₃]$^{2-}$ (**12**, 57–71%) have been prepared in good yield as Et₄N⁺ salts by reductive rearrangement reactions of the linear cluster [Fe₃S₄(Smes)₄]$^{3-}$ (**4**, Smes = mesitylthiolate(1−)) with Co(I) and Ni(0) reactants, respectively. (Et₄N)₂[**7**] crystallizes in orthorhombic space group *Pbcn* with *a* = 20.673 (3) Å, *b* = 16.600 (3) Å, *c* = 17.259 (2) Å, and *Z* = 4. (Et₄N)₂[NiFe₃S₄(PPh₃)(Smes)₃]·2MeCN was obtained in triclinic space group *P1̄* with *a* = 13.138 (3) Å, *b* = 15.461 (4) Å, *c* = 19.622 (4) Å, *α* = 107.12 (2)°, *β* = 94.54 (2)°, *γ* = 108.47 (2)°, and *Z* = 2. The crystal structures confirm the cubane-type structures and tetrahedral coordination at the M = Fe, Co, and Ni subsites of the [MFe₃S₄]$^{z+}$ cores. In **7**, the Co and Fe subsites are disordered and in **12** the phosphine ligand is bound to the Ni subsite. The clusters [NiFe₃S₄(Smes)₄]$^{3-}$ (**10**) and [Fe₄S₄(Smes)₄]$^{2-}$ (**6**) were obtained as an ca. 1:1 mixture by the reaction of Ni(AsPh₃)₄ and **4**. Potential and actual synthetic routes to [MFe₃S₄]$^{z+}$ clusters are outlined. The species **6, 7, 10** form a comparative set with equivalent structures and identical terminal ligands. These species and **12** are best distinguished by their ¹H NMR spectra which manifest contact-shifted resonances that are oppositely signed for substituents at the Fe and M = Co/Ni subsites. In **7**, the Fe subsites appear to be more reactive to ligand substitution by thiol than is the Co subsite; both subsites are substituted in the ligand redistribution system **5/7**. The three-member electron transfer series [CoFe₃S₄]$^{3+/2+/1+}$ and [NiFe₃S₄]$^{2+/1+/0}$ have been established. For the reversible couples [MFe₃S₄(Smes)₄]$^{2-/3-}$ the order of potentials is M = Fe < Co (0.18 V) < Ni (0.30 V), with the indicated potential differences vs M = Fe. Mössbauer spectroscopy reveals that **7** and the protein-bound [CoFe₃S₄]$^{2+}$ cluster of *D. gigas* ferredoxin II have equivalent electronic structures at 4.2 K. As judged by isomer shifts at 1.5 K, the [NiFe₃S₄]$^{1+}$ core of polycrystalline **12** contains three equivalent iron sites. However, the 4.2 K Mössbauer spectra obtained in strong applied magnetic fields show clearly that the three sites are magnetically distinct. Interestingly, the room temperature solution ¹H NMR data of **7** and **12** indicate equivalent sites. Isomer shifts imply the fragment formulations Co²⁺ (*S* = ³/₂) + [Fe₃S₄]⁰ (*S* = 2) and Ni²⁺ (S = 1) + [Fe₃S₄]¹⁻ (*S* = ⁵/₂), with antiparallel spin coupling affording the observed *S* = ¹/₂ and ³/₂ ground states, respectively. Comparison of the isomer shifts of the [NiFe₃S₄]¹⁺ core with those of other [MFe₃S₄]¹⁺ cubanes (M = Fe, Zn, Cd) suggests a shifted electron density from the [Fe₃S₄]¹⁻ fragment to the nickel site. The close correspondence of Mössbauer and EPR parameters of synthetic clusters (**7, 12**) with those of protein [CoFe₃S₄]²⁺ and [NiFe₃S₄]¹⁺ clusters indicates that the latter contain the tightly bound cubane-type structures established by X-ray diffraction for the synthetic species.

Introduction

The protein-bound cluster Fe₃S₄(S·Cys)₃ is now recognized, on the basis of its characteristic EPR, Mössbauer, and MCD spectroscopic properties, to occur in a relatively large number of iron–sulfur proteins and enzymes.[1,2] Its cuboidal structure **1**, illustrated in Table I, has been demonstrated by X-ray analysis of three proteins.[3–5] While the biological function (if any) of this cluster remains obscure, it possesses at least two properties of current significance in the field of metal clusters in biology. One of these involves reactivity and the second electronic structure.

Trinuclear cluster **1**, when in the [Fe₃S₄]$^{0,1-}$ core oxidation states, has a binding affinity for certain divalent metal ions that affords the cubane-type clusters **2**.[6–15] The situation is summarized in Table I, from which it is evident that ferredoxin proteins (note abbreviations) may be reconstituted in reaction 1 to a homometallic (Fe₄S₄) or to a heterometallic (MFe₃S₄) species. In the remaining known oxidation state of **1**, [Fe₃S₄]¹⁺, the electrophilic demands of three Fe³⁺ sites render the sulfur atoms insufficiently basic to bind divalent ions of the first transition series. Binding

(1) (a) Beinert, H.; Thomson, A. J. *Arch. Biochem. Biophys.* **1983**, *222*, 333. (b) Beinert, H.; Kennedy, M. C. *Eur. J. Biochem.* **1989**, *186*, 5. (c) Beinert, H. *FASEB J.* **1990**, *4*, 2483. (d) Cammack, R. *Adv. Inorg. Chem.* **1992**, *38*, 281.

(2) Holm, R. H. *Adv. Inorg. Chem.* **1992**, *38*, 1.

(3) Robbins, A. H.; Stout, C. D. *Proc. Natl. Acad. Sci. U.S.A.* **1989**, *86*, 3639; *Proteins* **1989**, *5*, 289.

(4) Stout, C. D. *J. Biol. Chem.* **1988**, *263*, 9256; *J. Mol. Biol.* **1989**, *205*, 545.

(5) (a) Kissinger, C. R.; Adman, E. T.; Sieker, L. C.; Jensen, L. H. *J. Am. Chem. Soc.* **1988**, *110*, 8721. (b) Kissinger, C. R.; Sieker, L. C.; Adman, E. T.; Jensen, L. H. *J. Mol. Biol.* **1991**, *219*, 693.

(6) (a) Kent, T. A.; Dreyer, J.-L.; Kennedy, M. C.; Huynh, B. H.; Emptage, M. H.; Münck, E. *Proc. Natl. Acad. Sci. U.S.A.* **1982**, *79*, 1096. (b) Beinert, H.; Emptage, M. H.; Dreyer, J.-L.; Scott, R. A.; Hahn, J. E.; Hodgson, K. O.; Thomson, A. J. *Proc. Natl. Acad. Sci. U.S.A.* **1983**, *80*, 393. (c) Kennedy, M. C.; Emptage, M. H.; Dreyer, J.-L.; Beinert, H. *J. Biol. Chem.* **1983**, *258*, 11098. (d) Emptage, M. H.; Dreyer, J.-L.; Kennedy, M. C.; Beinert, H. *J. Biol. Chem.* **1983**, *258*, 11106. (e) Kent, T. A.; Emptage, M. H.; Merkle, H.; Kennedy, M. C.; Beinert, H.; Münck, E. *J. Biol. Chem.* **1985**, *260*, 6871.

[†] Harvard University.
[§] Carnegie Mellon University.

Table I. Reconstitution of Protein-Bound Cuboidal Clusters to Cubane-Type Clusters

protein[a]	M[b]	structure (1)	reactions
aconitase	Fe^{2+}	3	6
Azotobacter vinelandii (*Av*) Fd I	Fe^{2+}	4	
Desulfovibrio africanus (*Da*) Fd III	Fe^{2+}, Zn^{2+}, Cd^{2+} Tl^{1+}		7–9
Desulfovibrio gigas (*Dg*) Fd II	Fe^{2+}, Co^{2+}, Zn^{2+}, Cd^{2+}	5	10–13
Pyrococcus furiosus (*Pf*) Fd	Fe^{2+}, Ni^{2+}		14, 15

[a] Fd = ferredoxin. [b] When more than one cluster **2** exists for a given protein, the incorporated metal M is included in the abbreviated designation (e.g., *Da* Fd III/Zn).

in this state is thus far restricted to the soft, thiophilic Tl^{1+} ion.[9] Terminal ligands L at the filled subsite have been identified as H_2O/OH^- in aconitase[16] and *Pf* Fd/Fe[17] but are uncertain in other cases. No other native metal–sulfur cluster is known to bind extrinsic metal ions.[18]

Cluster **1** in the $[Fe_3S_4]^{1+}$ state contains three high-spin Fe^{3+} sites that are indistinguishable by Mössbauer spectroscopy and antiferromagnetically coupled[19] to give an $S = {}^1/_2$ ground state. The $[Fe_3S_4]^0$ state has a unique electronic structure.[20] An Fe^{2+} ($S = 2$) ion and an Fe^{3+} ($S = {}^5/_2$) ion form a delocalized pair with parallel coupled spins whose resultant $S = {}^9/_2$ is antiparallel coupled to the spin ($S = {}^5/_2$) of an Fe^{3+} atom to give the system spin $S = 2$.[20] The $[Fe_3S_4]^{1-}$ state has been characterized only as its zinc cluster $[ZnFe_3S_4]^{1+}$ in *Dg* Fd II/Zn.[12] Reduction occurs primarily at the Fe^{3+} site, and the $S = {}^5/_2$ spin state arises from antiparallel coupling of $S = {}^9/_2$ and 2 (Fe^{2+}) spins. Electron distributions in clusters **1** and **2** have been deduced from ^{57}Fe isomer shifts in Mössbauer spectra.[1a,2,6a,e,10–13,20] Structures, reactivities, and electronic features of these clusters have been summarized.[2]

Some seven types of heterometal clusters have now been prepared. Those with M = V, Mo, W, Re,[2] and Nb[21] are obtained

in self-assembly systems containing the appropriate $[MS_4]^{2-}$ precursor. Clusters whose M component does not form a tetrathiometalate must be obtained by other routes. We have reported that reductive rearrangement of the linear Fe^{3+} cluster $[Fe_3S_4\text{-}(SEt)_4]^{3-}$[22] induced by reaction with Ni(0) affords $[NiFe_3Q_4]^{1+}$ clusters (Q = S, Se).[23,24] With coordinated thiolate as the apparent reductant, $[CoFe_3S_4]^{2+}$[25] and $[MoFe_3S_4]^0$[26] clusters have been prepared in related reactions.

We have augmented our investigation of heterometal cubane clusters with biological metals with several aims in mind. We wish to assess the scope of the reductive rearrangement process with differently substituted linear clusters and low-valent metal complexes, to improve the stability and provide further structural definition of the product MFe_3S_4 clusters, and to investigate reactivity properties at the M and Fe subsites. Additionally, we seek a more detailed examination of electronic features, especially electron distribution, in species with different terminal substituents and free of the potentially perturbative influence of protein structure and environment. Toward this end, we report the syntheses, structures, and leading properties of new clusters containing the $[CoFe_3S_4]^{2+}$ and $[NiFe_3S_4]^{1+}$ core oxidation levels and comparisons with features of a homometallic $[Fe_4S_4]^{2+}$ cluster with equivalent terminal ligation.

Experimental Section

Preparation of Compounds. All operations were performed under a pure dinitrogen atmosphere; solvents were dried by standard procedures and degassed prior to use. The compounds 2,4,6-trimethylbenzenethiol[27] (mesitylthiol, HSmes) and $(Et_4N)_3[Fe_3S_4(SEt)_4]$[22] were prepared as described. Sodium mesitylthiolate (Na(Smes)) was obtained from the reaction of 6.90 g (45.2 mmol) of the thiol with a solution of 1.81 g (45.1 mmol) of NaOH in 100 mL of methanol. Solvent removal yielded a white powder. ^1H NMR (CD_3CN): δ 2.08 (3, *p*-Me), 2.25 (6, *o*-Me), 6.61 (2, *m*-H). Impurity levels in the preparations of cluster compounds were assessed by ^1H NMR.

$(Et_4N)_3[Fe_3S_4(Smes)_4]$. To a solution of 2.72 g (17.8 mmol) of mesitylthiol in 150 mL of acetonitrile was added a solution of 4.15 g (4.46 mmol) of $(Et_4N)_3[Fe_3S_4(SEt)_4]$ in 50 mL of acetonitrile at 0 °C over a 10-min period. The reaction mixture was stirred for 1 h and the solvent was removed in vacuo to afford a shiny black solid. The ^1H NMR spectrum showed the product to be substantially pure, with a slight ($\leq 5\%$) contamination with $(Et_4N)_2[Fe_4S_4(Smes)_4]$[28] (vide infra). Recrystallization of 1.0 g of this material from acetonitrile by means of ether diffusion afforded 0.80 g of pure product as black microcrystals. ^1H NMR (CD_3CN, anion, 297 K): δ 43.7 (br, *m*-H), 48.8 (br, *o*-Me), 54.7 (br, *p*-Me). Absorption spectrum (acetonitrile): λ_{max} (ϵ_M) 341 (17900), 418 (17300), 519 (sh, 8600), 574 (sh, 7100), 743 (sh, 1800) nm. Anal. Calcd for $C_{60}H_{104}Fe_3N_3S_8$: C, 55.80; H, 8.12; Fe, 12.97; N, 3.25; S, 19.86. Found: C, 55.83; H, 8.15; Fe, 12.92; N, 4.29; S, 19.86.

$(Et_4N)_2[Fe_4S_4(Smes)_4]$. This compound has been reported,[28] but its preparation has not been described. To a solution of 2.00 g (2.34 mmol) of $(Et_4N)_2[Fe_4S_4(SEt)_4]$[22] in 150 mL of acetonitrile was added a solution of 1.43 g (9.39 mmol) of mesitylthiol. The mixture was stirred for 20 min, and volatiles were slowly removed in vacuo to give a shiny black solid residue. This material was recrystallized from acetonitrile/ether to afford 1.61 g (57%) of product as black crystals. Its ^1H NMR spectrum is shown in Figure 3. Absorption spectrum (acetonitrile): λ_{max} (ϵ_M) 343 (16200), 409 (20300) nm. Anal. Calcd for $C_{52}H_{84}Fe_4N_2S_8$: C, 51.31; H, 6.96; Fe, 18.35; N, 2.30; S, 21.07. Found: C, 51.27; H, 7.08; Fe, 18.31; N, 2.36; S, 21.02.

(7) George, S. J.; Armstrong, F. A.; Hatchikian, E. C.; Thomson, A. J. *Biochem. J.* **1989**, *264*, 275.

(8) Butt, J. N.; Armstrong, F. A.; Breton, J.; George, S. J.; Thomson, A. J.; Hatchikian, E. C. *J. Am. Chem. Soc.* **1991**, *113*, 6663.

(9) Butt, J. N.; Sucheta, A.; Armstrong, F. A.; Breton, J.; Thomson, A. J.; Hatchikian, E. C. *J. Am. Chem. Soc.* **1991**, *113*, 8948.

(10) Moura, J. J. G.; Moura, I.; Kent, T. A.; Lipscomb, J. D.; Huynh, B. H.; LeGall, J.; Xavier, A. V.; Münck, E. *J. Biol. Chem.* **1982**, *257*, 6259.

(11) Moura, I.; Moura, J. J. G.; Münck, E.; Papaefthymiou, V.; LeGall, J. *J. Am. Chem. Soc.* **1986**, *108*, 349.

(12) Surerus, K. K.; Münck, E.; Moura, I.; Moura, J. J. G.; LeGall, J. *J. Am. Chem. Soc.* **1987**, *109*, 3805.

(13) Münck, E.; Papaefthymiou, V.; Surerus, K. K.; Girerd, J.-J. In *Metal Ions in Proteins*; Que, L., Jr., Ed.; ACS Symp. Ser. 372; American Chemical Society: Washington, DC, 1988; Chapter 15.

(14) Conover, R. C.; Kowal, A. T.; Fu, W.; Park, J.-B.; Aono, S.; Adams, M. W. W.; Johnson, M. K. *J. Biol. Chem.* **1990**, *265*, 8533.

(15) Conover, R. C.; Park, J.-B.; Adams, M. W. W.; Johnson, M. K. *J. Am. Chem. Soc.* **1990**, *112*, 4562.

(16) Werst, M. M.; Kennedy, M. C.; Beinert, H.; Hoffman, B. M. *Biochemistry* **1990**, *29*, 10526.

(17) Park, J.-B.; Fan, C.; Hoffman, B. M.; Adams, M. W. W. *J. Biol. Chem.* **1991**, *266*, 19351.

(18) However, a close non-biological parallel to reaction 1 is found in the reaction of metals with $[Mo_3S_4(OH_2)_9]^{4+}$ to afford the heterometal cubanes $[MMo_3S_4]^{4+}$: Shibahara, T. *Adv. Inorg. Chem.* **1991**, *37*, 143.

(19) Kent, T. A.; Huynh, B.-H.; Münck, E. *Proc. Natl. Acad. Sci. U.S.A.* **1980**, *77*, 6574.

(20) Papaefthymiou, V.; Girerd, J.-J.; Moura, I.; Moura, J. J. G.; Münck, E. *J. Am. Chem. Soc.* **1987**, *109*, 4703.

(21) Li, J.; Lee, S. C.; Holm, R. H. Unpublished results.

(22) Hagen, K. S.; Watson, A. D.; Holm, R. H. *J. Am. Chem. Soc.* **1983**, *105*, 3905.

(23) Ciurli, S.; Yu, S.-B.; Holm, R. H.; Srivastava, K. K. P.; Münck, E. *J. Am. Chem. Soc.* **1990**, *112*, 8169.

(24) Ciurli, S.; Ross, P. K.; Scott, M. J.; Yu, S.-B.; Holm, R. H. *J. Am. Chem. Soc.* **1992**, *114*, 5415.

(25) Roth, E. K. H.; Greneche, J. M.; Jordanov, J. *J. Chem. Soc., Chem. Commun.* **1991**, 105. Stib = 2,4,6-triisopropylbenzenethiolate(1–).

(26) (a) Coucouvanis, D.; Al-Ahmad, S.; Salifoglou, A.; Dunham, W. R.; Sands, R. H. *Angew. Chem., Int. Ed. Engl.* **1988**, *27*, 1353. (b) Coucouvanis, D.; Al-Ahmad, S.; Salifoglou, A.; Papaefthymiou, V.; Kostikas, A.; Simopoulos, A. *J. Am. Chem. Soc.* **1992**, *114*, 2472.

(27) Chisholm, M.; Corning, J. F.; Huffman, J. C. *Inorg. Chem.* **1984**, *23*, 754.

(28) (a) Ueyama, N.; Terakawa, T.; Sugawara, T.; Fuji, M.; Nakamura, A. *Chem. Lett.* **1984**, 1287. (b) Ueyama, N.; Sugawara, T.; Fuji, M.; Nakamura, A.; Yasuoka, N. *Chem. Lett.* **1985**, 175.

Table II. Crystallographic Data[a] for (Et₄N)₂[CoFe₃S₄(Smes)₄] ((Et₄N)₂[7]) and (Et₄N)₂[NiFe₃S₄(PPh₃)(Smes)₃]·2MeCN ((Et₄N)₂[12]·2MeCN)

	(Et₄N)₂[7]	(Et₄N)₂[12]·2MeCN
formula	C₅₂H₈₄CoFe₃N₂S₈	C₆₅H₉₄Fe₃N₄NiPS₇
formula wt	1220.2	1413.1
crystal system	orthorhombic	triclinic
space group	*Pbcn*	*P1̄*
Z	4	2
a, Å	20.673 (3)	13.138 (3)
b, Å	16.600 (3)	15.461 (4)
c, Å	17.259 (2)	19.622 (4)
α, deg		107.12 (2)
β, deg		94.54 (2)
γ, deg		108.47 (2)
V, Å³	5923 (2)	3547.1 (13)
*d*ₐₗ꜀, g/cm³	1.37	1.32
T, K	233	233
μ, cm⁻¹	16.0	11.3
R,[b] *R*ᵥᵥ[c] (%)	6.24, 5.95	6.89, 7.21

[a] All data collected with Mo Kα radiation (λ = 0.71069 Å). [b] $R = \sum ||F_o| - |F_c||/\sum|F_o|$. [c] $R_w = \{\sum[w(|F_o| - |F_c|)^2]/\sum[w|F_o|^2]\}^{1/2}$.

(Et₄N)₂[CoFe₃S₄(Smes)₄]. To a vigorously stirred slurry of 1.46 g (11.2 mmol) of CoCl₂ in 100 mL of acetonitrile was added 4.16 g (33.5 mmol) of trimethyl phosphite, resulting in a color change to dark blue. Zinc metal powder (0.37 g, 5.6 mmol) was added and the reaction mixture was stirred for 3 h, whereupon a dark green color developed. The mixture was filtered and the solvent removed in vacuo to afford Co(P-(OMe)₃)₃Cl as a dark green solid. ¹H NMR (CD₃CN): δ 3.62. (The related compounds Co(PR₃)₃X (X = halide) have been prepared earlier.[29]) A solution of 0.97 g (2.07 mmol) of Co(P(OMe)₃)₃Cl was added to a solution of 0.36 g (2.08 mmol) of Na(Smes) in 20 mL of methanol. The color of the solution rapidly changed to dark brown owing to the formation of Co(P(OMe)₃)₃(Smes). (This compound was isolated in a separate experiment as a dark brown solid. ¹H NMR (CD₃CN): δ 3.62 (OMe), 29.0 (br, *m*-H), 40.0 (br, *o*-Me), 45.8 (br, *p*-Me).) THF (100 mL) was added and the solution was filtered and cooled to 0 °C. A solution of 0.45 g (0.35 mmol) of (Et₄N)₃[Fe₃S₄(Smes)₄] in 100 mL of acetone was slowly added, and the reaction mixture was stirred at 0 °C for 2 h. At this point the product consisted of an ca. 98/2 mixture of the Et₄N⁺ salts of [CoFe₃S₄(Smes)₄]²⁻ and [Fe₄S₄(Smes)₄]²⁻. Ether (300 mL) was layered on the acetonitrile solution, which was maintained at −20 °C for 2 days. The product was collected by filtration as 0.340 g (80%) of red-black crystals which contained ≤2% of Fe₄S₄ impurity by ¹H NMR. Absorption spectrum (acetonitrile): λₘₐₓ (ε_M) 330 (10 000), 421 (14 000) nm. Anal. Calcd for C₅₂H₈₄CoFe₃N₂S₈: C, 51.18; H, 6.94; Co, 4.83; Fe, 13.73; N, 2.30; S, 21.02. Found: C, 50.66; H, 6.98; Co, 4.84; Fe, 13.93; N, 2.36; S, 21.32.

(Et₄N)₃[NiFe₃S₄(Smes)₄]. A solution of 0.500 g (0.387 mmol) of (Et₄N)₃[Fe₃S₄(Smes)₄] in 100 mL of acetonitrile was added to a solution of 0.522 g (0.407 mmol) of Ni(AsPh₃)₄[30] in 50 mL of acetonitrile. The reaction mixture was stirred at room temperature for 2 h. Ether was layered on the solution and the mixture was maintained at −20 °C for 2 days. The black microcrystalline solid was collected and found to consist of an equimolar mixture of the desired product and (Et₄N)₂-[Fe₄S₄(Smes)₄]. The mixture proved suitable for characterization of ¹H NMR and electrochemical properties of the NiFe₃S₄ cluster.

(Et₄N)₂[NiFe₃S₄(PPh₃)(Smes)₃]·MeCN. A solution of 1.00 g (0.774 mmol) of (Et₄N)₃[Fe₃S₄(Smes)₄] in 100 mL of acetonitrile was added to a solution of 0.943 g (0.851 mmol) of Ni(PPh₃)₄[30] in 50 mL of acetonitrile. The reaction mixture was stirred for 10 min. Ether (300 mL) was layered on the solution, which was maintained at −20 °C for 2 days. The product was collected by filtration as 0.728 g (71%) of a black crystalline solid which contained less than 2% of Fe₄S₄ contaminant. Absorption spectrum (acetonitrile): λₘₐₓ (ε_M) 337 (10 300), 386 (10 200) nm. Analytical data most satisfactorily corresponded to an acetonitrile monosolvate. Anal. Calcd for C₆₃H₉₁Fe₃N₃NiPS₇: C, 55.15; H, 6.68; Fe, 12.21; N, 3.06; Ni, 4.28; P, 2.26; S, 16.37. Found: C, 54.23; H, 6.50; Fe, 12.71; N, 3.20; Ni, 4.38; P, 2.35; S, 16.68. The compound was also prepared in 58% yield in a reaction of the same scale employing Ni-(PPh₃)₃(PhCN)[31] as a reactant.

Table III. Selected Interatomic Distances (Å) and Bond Angles (deg) for (Et₄N)₂[CoFe₃S₄(Smes)₄]

Distances[a]			
M–M	2.725→2.772	M–S꜀ₒᵣₑ	2.250→2.286
mean	2.75 (2)	mean	2.27 (2)
M–S(5)	2.252 (2)		
M–S(6)	2.257 (2)		

Angles			
M–M–M	59.2→60.5	M–S꜀ₒᵣₑ–M	73.8→75.3
mean	60.0 (5)	mean	74.6 (6)
S꜀ₒᵣₑ–M–S꜀ₒᵣₑ	102.6→104.3	S꜀ₒᵣₑ–M–Sₜₕᵢₒₗₐₜₑ	111.4→120.7
mean	103.5 (8)	mean	115 (4)
M–S(5)–C(11)	99.6 (3)		
M–S(6)–C(21)	99.4 (3)		

[a] M = Co, Fe.

Chart I

[Fe₃S₄(SEt)₄]³⁻ (**3**)	[CoFe₃S₄(Stib)₄]²⁻ (**8**)
[Fe₃S₄(Smes)₄]³⁻ (**4**)	[NiFe₃S₄(SEt)₄]³⁻ (**9**)
[Fe₄S₄(SEt)₄]²⁻ (**5**)	[NiFe₃S₄(Smes)₄]³⁻ (**10**)
[Fe₄S₄(Smes)₄]²⁻ (**6**)	[NiFe₃S₄(PPh₃)(SEt)₃]²⁻ (**11**)
[CoFe₃S₄(Smes)₄]²⁻ (**7**)	[NiFe₃S₄(PPh₃)(Smes)₃]²⁻ (**12**)

X-ray Data Collection and Reduction. Black crystals of (Et₄N)₂-[CoFe₃S₄(Smes)₄] and (Et₄N)₂[NiFe₃S₄(PPh₃)(Smes)₃]·2MeCN were grown by vapor diffusion of ether into acetonitrile solutions. Single crystals were coated with grease and attached to glass fibers. The crystals were transferred to a Nicolet R3 diffractometer and cooled with a stream of cold dinitrogen. Experimentals details of the data collections are included in Table II.

Lattice parameters were obtained from a least-squares analysis of 25 machine-centered reflections with 20° ≤ 2θ ≤ 30°. Decay corrections were based on the measured intensities of three reflections monitored periodically throughout the course of the data collections; neither compound showed significant decay. The raw intensity data were converted to structure factor amplitudes and their esd's by corrections for scan speed, background, and Lorentz and polarization effects using the program XDISK of the SHELXTL PLUS program package. Empirical absorption corrections based on the observed variations in intensity of azimuthal (Ψ) scans were applied using the program XEMP. (Et₄N)₂-[CoFe₃S₄(Smes)₄] crystallizes in orthorhombic space group *Pbcn*, which was identified by systematic absences. (Et₄N)₂[NiFe₃S₄(PPh₃)-(Smes)₃]·2MeCN crystallizes in the triclinic system, and statistics identified the space group as *P1̄*. Crystallographic data are listed in Table II.

Structure Solutions and Refinements. Structures were solved by direct methods and were refined by means of standard least-squares and Fourier techniques. Hydrogen atoms were assigned idealized locations and were given the uniform value B_{iso} = 0.8 Å². The asymmetric unit of (Et₄N)₂[CoFe₃S₄(Smes)₄] consists of one-half anion and one cation. No unique site could be found for the cobalt atom, and the cluster was refined with metal subsite occupancies of 0.75 Fe and 0.25 Co. All non-hydrogen atoms were refined anisotropically except for the disordered metal atoms. The asymmetric unit of (Et₄N)₂[NiFe₃S₄(PPh₃)-(Smes)₃]·2MeCN consists of one anion, one full cation, two half-cations, and two acetonitrile solvate molecules. The α-carbon atoms of the two half-cations are disordered across inversion centers; the two unique positions located for each atom were refined with a site occupancy of 0.5. All non-hydrogen atoms of the anion were refined anisotropically. In the last cycle of refinement of both structures, all parameters shifted by <1% of the esd of the parameter, and final difference Fourier maps showed no significant electron density. Selected interatomic distances and angles of the two structures are collected in Tables III and IV.[32]

Other Physical Measurements. Spectrophotometric, ¹H NMR, EPR and Mössbauer spectroscopic, electrochemical, and magnetic measurements were performed under anaerobic conditions using the equipment and procedures described elsewhere.[24,33,34] Potentials were determined with use of a Pt working electrode and are reported vs the SCE. Isomer shifts of ⁵⁷Fe are referenced to iron metal at room temperature.

(29) (a) Aresta, M.; Rossi, M.; Sacco, A. *Inorg. Chim. Acta* **1969**, *3*, 227. (b) Klein, H.-F.; Karsch, H. H. *Chem. Ber.* **1975**, *108*, 944. (c) Baysdon, S. L.; Liebeskind, L. S. *Organometallics* **1982**, *1*, 771.

(30) Ittel, S. D. *Inorg. Synth.* **1990**, *28*, 102.

(31) Bassi, I. W.; Benedicenti, C.; Calcaterra, M.; Rucci, G. *J. Organomet. Chem.* **1976**, *117*, 285.

(32) See the paragraph at the end of this article concerning supplementary material available.

(33) Zimmermann, R.; Münck, E.; Brill, W. J.; Shah, V. K.; Henzl, M. T.; Rawlings, J.; Orme-Johnson, W. H. *Biochim. Biophys. Acta* **1978**, *537*, 185.

(34) Ciurli, S.; Carrié, M.; Weigel, J. A.; Carney, M. J.; Stack, T. D. P.; Papaefthymiou, G. C.; Holm, R. H. *J. Am. Chem. Soc.* **1990**, *112*, 2654.

10846 *J. Am. Chem. Soc., Vol. 114, No. 27, 1992*

Zhou et al.

Table IV. Selected Interatomic Distances (Å) and Bond Angles (deg) for $[NiFe_3S_4(PPh_3)(Smes)_3]^{2-}$

Distances			
Ni(1)–Fe(1)	2.693 (2)	Fe(1)–Fe(2)	2.704 (2)
Ni(1)–Fe(2)	2.665 (2)	Fe(1)–Fe(3)	2.765 (2)
Ni(1)–Fe(3)	2.668 (1)	Fe(2)–Fe(3)	2.797 (2)
mean	2.68 (2)	mean	2.75 (5)
Ni(1)–S(1)	2.272 (3)	Fe(1)–S(4)	2.327 (3)
Ni(1)–S(2)	2.283 (3)	Fe(2)–S(4)	2.295 (2)
Ni(1)–S(3)	2.265 (3)	Fe(3)–S(4)	2.302 (3)
mean	2.273 (9)	mean	2.31 (2)
Ni(1)–P(1)	2.181 (3)	Fe(1)–S(2)	2.277 (4)
		Fe(1)–S(3)	2.266 (3)
Fe(1)–S(5)	2.278 (3)	Fe(2)–S(1)	2.272 (3)
Fe(2)–S(6)	2.286 (4)	Fe(2)–S(3)	2.283 (3)
Fe(3)–S(7)	2.289 (3)	Fe(3)–S(1)	2.274 (3)
mean	2.284 (6)	Fe(3)–S(2)	2.292 (3)
		mean	2.277 (9)

Angles			
S(1)–Ni(1)–S(2)	107.0 (1)	S(4)–Fe(1)–S(5)	105.2 (1)
S(1)–Ni(1)–S(3)	106.3 (1)	S(4)–Fe(2)–S(6)	112.9 (1)
S(2)–Ni(1)–S(3)	104.0 (1)	S(4)–Fe(3)–S(7)	122.4 (1)
Fe(1)–Ni(1)–Fe(2)	60.6 (1)	S(2)–Fe(1)–S(3)	104.2 (1)
Fe(1)–Ni(1)–Fe(3)	62.1 (1)	S(1)–Fe(2)–S(3)	105.7 (1)
Fe(2)–Ni(1)–Fe(3)	63.3 (1)	S(1)–Fe(3)–S(2)	106.6 (1)
Ni(1)–Fe(1)–Fe(2)	59.2 (1)	S(2)–Fe(1)–S(4)	103.7 (1)
Ni(1)–Fe(1)–Fe(3)	58.5 (1)	S(3)–Fe(1)–S(4)	105.9 (1)
Ni(1)–Fe(2)–Fe(1)	60.2 (1)	S(1)–Fe(2)–S(4)	101.4 (1)
Ni(1)–Fe(2)–Fe(3)	58.4 (1)	S(3)–Fe(2)–S(4)	106.4 (1)
Ni(1)–Fe(3)–Fe(1)	59.4 (1)	S(1)–Fe(3)–S(4)	101.1 (1)
Ni(1)–Fe(3)–Fe(2)	58.3 (1)	S(2)–Fe(3)–S(4)	104.0 (1)
Ni(1)–S(1)–Fe(2)	71.8 (1)	Fe(2)–S(1)–Fe(3)	75.9 (1)
Ni(1)–S(1)–Fe(3)	71.9 (1)	Fe(1)–S(2)–Fe(3)	74.5 (1)
Ni(1)–S(2)–Fe(1)	72.4 (1)	Fe(1)–S(3)–Fe(2)	72.9 (1)
Ni(1)–S(2)–Fe(3)	71.3 (1)	Fe(1)–S(4)–Fe(2)	71.6 (1)
Ni(1)–S(3)–Fe(1)	72.9 (1)	Fe(1)–S(4)–Fe(3)	73.3 (1)
Ni(1)–S(3)–Fe(2)	71.8 (1)	Fe(2)–S(4)–Fe(3)	74.9 (1)
Fe(1)–Ni(1)–P(1)	140.8 (1)	S(1)–Ni(1)–P(1)	115.9 (1)
Fe(2)–Ni(1)–P(1)	152.8 (1)	S(2)–Ni(1)–P(1)	103.7 (1)
Fe(3)–Ni(1)–P(1)	135.5 (1)	S(3)–Ni(1)–P(1)	118.7 (1)

Results and Discussion

The clusters **3–12** listed below are of principal interest in this work. The structure of cluster **6**[28b] has been described, as have the preparations and certain properties of **8**.[25] Clusters **9** and **11** were the subjects of our initial reports on $[NiFe_3Q_4]^{1+}$ clusters (Q = S, Se)[23,24] while **4, 7, 10,** and **12** are new species. Note that **6, 7,** and **10** form a comparative set in that all subsites of the MFe_3S_4 cores (M = Fe, Co, Ni) have identical (mesitylthiolate) ligands, and **12** differs from these only in having a PPh_3 ligand at the nickel subsite. The comparative features of this unique set of clusters will be addressed in the sections that follow.

Cluster Synthesis. When the self-assembly route to MFe_3S_4 clusters cannot be pursued owing to the unavailability of the appropriate $[MS_4]^{2-}$ precursor, the generalized reactions 2–4 in Table V may be considered. The trinuclear linear clusters **3** and **4** contain three Fe^{3+} ions in the $[Fe_3S_4]^{1+}$ core **13**. They are potentially subject to cubane-type cluster formation upon metal-induced rearrangement to a cuboidal geometry equivalent to **1** by reaction with some generalized species M^zL_n. These reactions are ones of *fragment condensation*, with rearranged Fe_3S_4 being a fragment of the product cluster. The latter are written in terms of core and metal oxidation states inasmuch as the identity of the ligand at the M subsite cannot always be predicted, the formation of **9** and **11** in the same reaction system[23,24] being an example. The simplest of these reactions is 2, in which a strongly thiophilic metal induces rearrangement of the trinuclear cluster and is incorporated in the cluster with no change in redox state of either reactant. While seemingly plausible, no such reaction has yet been described. In reaction 3, the initial cluster is reduced by one electron and captures the metal without necessarily changing the oxidation state of M^z. In the examples given, added thiolate was

the reductant in the system affording **5**, whereas the apparent reductant in the formation of **8**[35] and the $MoFe_3S_4$ cluster[26] is coordinated thiolate. In reaction 4, a reduced metal source reduces the initial cluster, which reverts to a cuboidal form and captures the oxidized metal. This reaction type, termed *reductive rearrangement*, may be likened to inner-sphere electron transfer in which there is a persistent intermediate that closely resembles the final product.

Potentially more efficacious than reactions 2–4 is fragment condensation reaction 5 (Table V). Here preformed oxidized or reduced cuboidal core **14** binds metals in reactions analogous to reaction 1 (Table I). Thiophilic metals could bind $[Fe_3S_4]^{1+}$ in a non-redox process, as with *Da* Fd III/Tl.[9] Of more general value would be reactions of this oxidation state with reducing metals or binding of metals by $[Fe_3S_4]^0$ in a non-redox or one-electron reduction process. In the one possible case of this reaction,[25] oxidation of $[Fe_4S_4(Stib)_4]^{2-}$ affords an unstable $[Fe_3S_4]^{1+}$ species which with $CoCl_2$ yields a $[CoFe_3S_4]^{2+}$ cluster.[36] Unfortunately, reaction 5 is at present not practicable because no stable cuboidal cluster has been directly prepared nor have we found conditions which effect a linear → cuboidal rearrangement in the absence of added metal.[37]

The synthesis of cubane clusters studied in this work is summarized in Figure 1. Cluster **6** was obtained from **5** by a standard ligand substitution procedure. Clusters **7, 10,** and **12** were prepared by reductive rearrangement reaction 4 utilizing linear cluster **4**, obtained in 80% yield by ligand substitution of **3**, and Co(I) and Ni(0) precursors, respectively. The bulky mesitylthiolate ligand offers considerable advantages over ethanethiolate used in our previous synthesis of $NiFe_3S_4$ clusters.[23,24] Cluster **12** can be routinely obtained in purified yields of 70% or higher whereas multiple preparations of **11** resulted in yields of ca. 30% and were always accompanied by substantial quantities of Fe_4S_4 cluster **5**. Both **7** and **12** can be prepared such that virtually no **6** is present in the crude product and can be recrystallized without further formation of this cluster. Anaerobic solutions of **11** over about a day or longer tend to decompose, one product being **5**. Solutions of **12**, and also of **7**, are considerably more stable.

In the reaction system $3/Ni(PPh_3)_4$, clusters **9** and **11** are both formed.[24] The former presumably arises from EtS^-/PPh_3 ligand substitution of **11**. In contrast, **12** was the sole cluster product detected in an analogous reaction system, apparently because $mesS^-$ is an insufficiently strong nucleophile to displace PPh_3. This was verified by a separate experiment in which **12** was treated with 5 equiv of $(Et_4N)(Smes)$ in acetonitrile solution for 2 days. No reaction was observed. However, in the reaction of **4** with $Ni(AsPh_3)_4$, clusters **6** and **10** are formed in equimolar amounts. While the means of formation of **6** is obscure (as is that of **5** in related systems[24]), it would appear likely that **10** is the result of a substitution reaction of $[NiFe_3S_4(AsPh_3)(Smes)_3]^{2-}$ with thiolate. The lability order $AsPh_3 > PPh_3$ is not unexpected. The preparation of **10** completes the comparative set **6, 7,** and **10**. We have not found a means of cleanly separating **6** and **10**; however, the mixture suffices for determination of the ^1H NMR spectrum and redox potentials.

Mesitylthiolate clusters **6, 7,** and **12** may be recognized by their absorption spectra, shown in Figure 2. While these spectra cannot be interpreted in any detail, the bands, as those for the extensively studied $[Fe_4S_4(SR)_4]^{2-}$ clusters, doubtless arise from S → core charge transfer transitions. We note that the all-thiolate clusters **6** and **7** are distinguishable, in terms of both absorption maxima

(35) The claim[25] that cluster **8** is generated in quantitative yield in a reaction performed anaerobically cannot be correct if coordinated thiolate is the reductant. No exogenous reductant was specified.

(36) The reaction was carried out aerobically but the formation of $[CoFe_3S_4]^{2+}$ requires a reductant. The trinuclear species has been detected at low temperature by EPR: Roth, E. K. H.; Jordanov, J. *Inorg. Chem.* **1992,** *31,* 240.

(37) The reverse rearrangement has been observed upon unfolding inactive aconitase at high pH: Kennedy, M. C.; Kent, T. A.; Emptage, M.; Merkle, H.; Beinert, H.; Münck, E. *J. Biol. Chem.* **1984,** *259,* 14463. One implication of these results is that in the presence of sufficient thiolate ligands, the cuboidal form is metastable or unstable with respect to the linear form.
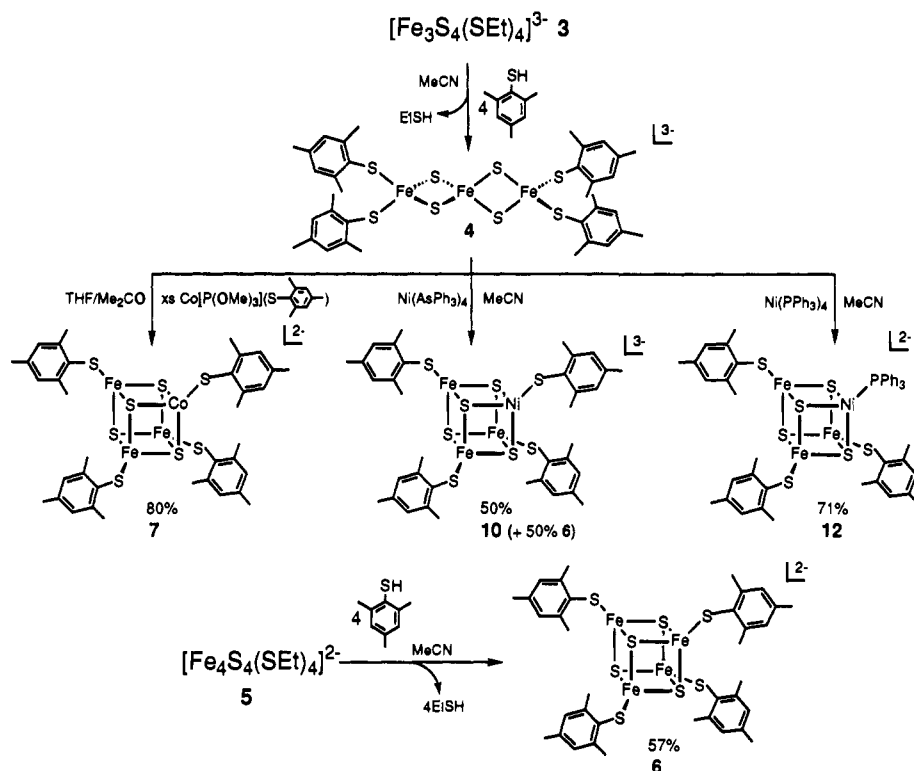
Figure 1. Synthesis of the heterometal cubane-type clusters [CoFe₃S₄(Smes)₄]²⁻ (**7**) and [NiFe₃S₄(PPh₃)(Smes)₃]²⁻ (**12**) by reductive rearrangement of [Fe₃S₄(Smes)₄]³⁻ (**4**) using Co(I) and Ni(0) reductants, respectively. Purified yields are indicated.
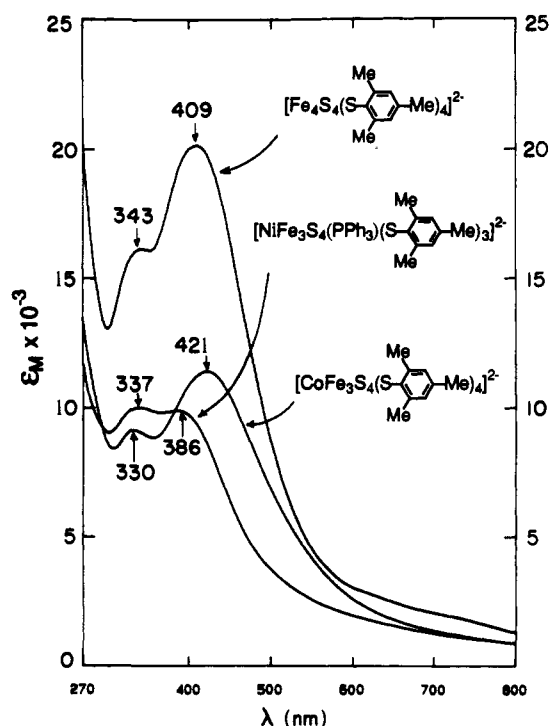

Figure 2. UV-visible absorption spectra of [MFe₃S₄(Smes)₄]²⁻ (M = Fe, Co) and [NiFe₃S₄(PPh₃)(Smes)₃]²⁻ in acetonitrile solutions; absorption maxima are indicated.

Figure 3. ¹H NMR spectra of [MFe₃S₄(Smes)₄]²⁻ (M = Fe, Co) and [NiFe₃S₄(PPh₃)(Smes)₃]²⁻ in acetonitrile solutions at 297 K; signal assignments are indicated.

and intensities. Even more diagnostic are the isotropically shifted ¹H NMR spectra, which are shown in Figure 3 and are considered below.

Cluster Structures. (a) **[CoFe₃S₄(Smes)₄]²⁻.** The crystal structure of (Et₄N)₂[7] is isomorphous with that of (Et₄N)₂[6];²⁸ᵇ the structure of the cluster is depicted in Figure 4. Metric values, some of which are listed in abbreviated form in Table III, and conformations of the mesityl substituents are essentially identical. The latter are directed outward from core faces and do not appear
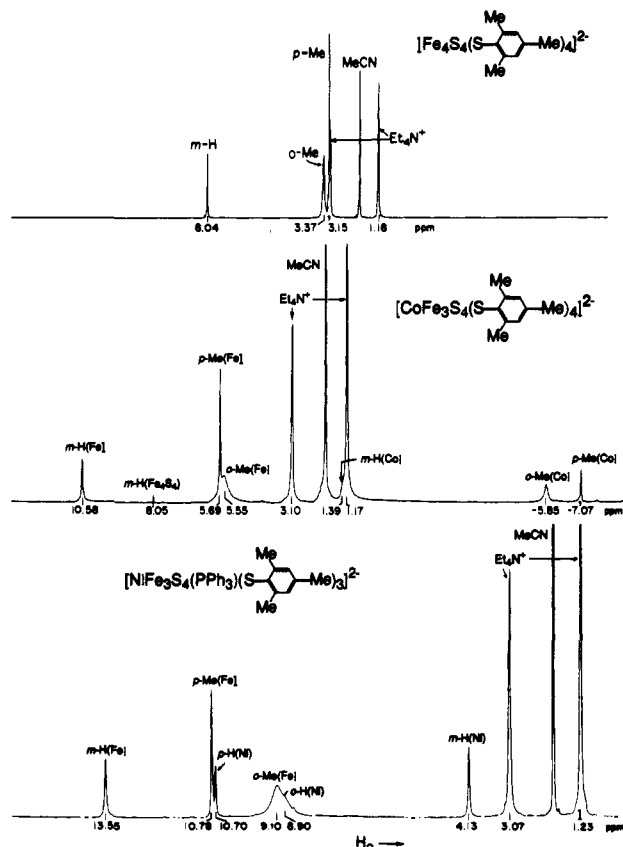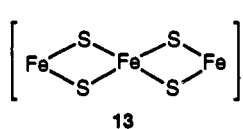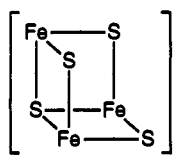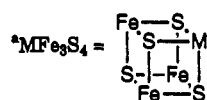
to exhibit any special interactions with the core. Cluster **7** has an imposed C₂ axis passing through the core faces M(1,1′)S(1,1′) and M(2,2′)S(2,2′). These results confirm the cubane-type structure of **7** but, because of the disordered metal sites, the

Table V. Synthesis of MFe₃S₄ᵃ Cubane Clusters by Fragment Condensation

reaction	Mᶻ	product	ref.
		b	---
	Fe²⁺	[Fe₄S₄(SEt)₄]²⁻ (5)	22
	Co²⁺	[CoFe₃S₄(Stib)₄]²⁻ (8)	25, c
	Mo⁰	[MoFe₃S₄(CO)₃(SEt)₃]³⁻	26
	Co¹⁺	[CoFe₃S₄(Smes)₄]²⁻ (7)	d
	Ni⁰	[NiFe₃S₄(SEt)₄]³⁻ (9)	23,24
	Ni⁰	[NiFe₃S₄(PPh₃)(SR)₃]²⁻ (R = Et, mes) (11,12)	23,24,d
	Co²⁺	[CoFe₃S₄(Stib)₄]²⁻ (8)	25

ᵃMFe₃S₄ =   [Fe—S / S—M / S—Fe / Fe—S structure]   ᵇNo examples of this reaction. ᶜ*Cf.* footnote 35. ᵈThis work.
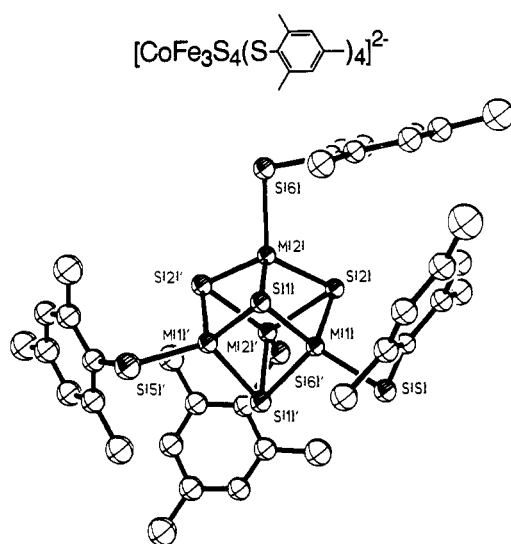
[CoFe₃S₄(S—⟨⟩—)₄]²⁻

Figure 4. Structure of [CoFe₃S₄(Smes)₄]²⁻ showing 30% probability ellipsoids and the atom labeling scheme. Primed and unprimed atoms are related by a C₂ axis; the metal sites M = Fe, Co are disordered.

structure cannot be analyzed in detail. We note, however, that the mean Fe–S terminal distance of 2.255 Å is marginally shorter that the corresponding value of 2.274 Å for **6**,[28b] implying a mean oxidation state no less than $Fe^{2.50+}$ in the [CoFe₃S₄]²⁺ core. This follows from a large body of structural data for Fe₄S₄ clusters that clearly demonstrates that terminal Fe–S distances decrease as the mean oxidation state of the core increases.[38]

(b) [NiFe₃S₄(PPh₃)(Smes)₃]²⁻. The compound (Et₄N)₂[**12**]·2MeCN crystallizes with no symmetry imposed on its cluster whose cubane-type structure, shown in Figure 5, approaches idealized C₃ symmetry. The main deviations within the [NiFe₃S₄]¹⁺ core are found with Fe–Fe distances, whose mean is 2.75 (5) Å. The angles Fe–Ni–P, S–Ni–P, and S(4)–Fe–S and phenyl ring relative orientations show substantial variations from
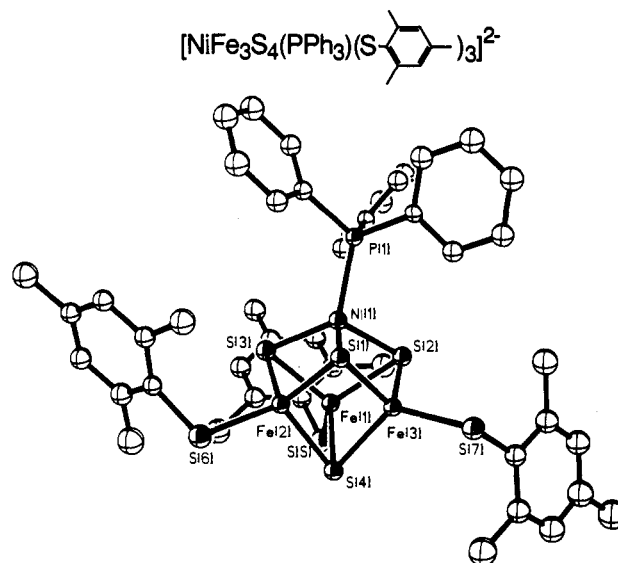
[NiFe₃S₄(PPh₃)(S—⟨⟩—)₃]²⁻

Figure 5. Structure of [NiFe₃S₄(PPh₃)(Smes)₃]²⁻ showing 30% probability ellipsoids and the atom labeling scheme.

C₃ symmetry. Large ranges of angles involving terminal ligands are commonly found with Fe₄S₄ clusters; there, as here, the origin must be crystal packing effects. Otherwise, the structure of **12** is dimensionally equivalent to that of **11**, which was reported earlier.[24] The mean Fe–S terminal bond length of 2.284 (6) Å is indistinguishable from that of **11**, but it is longer than that of **7**, implying that the Fe₃S₄ core fragment is somewhat more reduced. We shall return to the matter of charge distribution in a subsequent section.

Lastly, we are unable to discern clearly from these solid state structures the function of the mesityl vs smaller substituents in promoting cluster stability. However, the evidence is now incontrovertible that bulky substituents,[28a,38b,39] or incorporation of Fe₄S₄ cores into sterically protective macrocyclic structures,[40] can

(38) (a) Berg, J. M.; Holm, R. H. In *Iron–Sulfur Proteins*; Spiro, T. G., Ed.; Wiley-Interscience: New York, 1982; Chapter 1. (b) O'Sullivan, T.; Millar, M. M. *J. Am. Chem. Soc.* **1985**, *107*, 4096. (c) Carney, M. J.; Papaefthymiou, G. C.; Spartalian, K.; Frankel, R. B.; Holm, R. H. *J. Am. Chem. Soc.* **1988**, *110*, 6084 and references therein.

(39) (a) Mascharak, P. K.; Hagen, K. S.; Spence, J. T.; Holm, R. H. *Inorg. Chim. Acta* **1983**, *80*, 157. (b) Nakamoto, M.; Tanaka, K.; Tanaka, T. *J. Chem. Soc., Chem. Commun.* **1988**, 1422.

(40) Tomohiro, T.; Uoto, K.; Okuno, H. *J. Chem. Soc., Dalton Trans.* **1990**, 2459; *Chem. Express* **1990**, *5*, 37.

Table VI. ¹H Isotropic Shifts of MFe₃S₄ Clusters (M = Fe, Co, Ni) in CD₃CN Solutions at 297 K

| cluster | M site | $(\Delta H/H_0)_{iso}$,[a] ppm | | |
		o-Me/H	m-H	p-Me/H
[Fe₄S₄(Smes)₄]²⁻	Fe	−1.12	−1.43	−1.07
[CoFe₃S₄(Smes)₄]²⁻	Co	+8.10	+5.22	+9.15
	Fe	−3.30	−3.97	−3.61
[NiFe₃S₄(Smes)₄]³⁻	Ni	+5.77	+5.31	+8.18
	Fe	−7.81	−6.80	−9.38
[NiFe₃S₄(PPh₃)(Smes)₃]²⁻	Ni	−1.60	+3.17	−4.40
	Fe	−6.85	−6.94	−8.70

[a] $(\Delta H/H_0)_{iso} = (\Delta H/H_0)_{dia} - (\Delta H/H_0)_{obs}$; diamagnetic references are (Et₄N)(Smes) and PPh₃.

Table VII. Fragment Formulations of Heterometal Cubane Cores [MFe₃S₄]²⁺ (M = Fe, Co, Ni, Zn, Cd)

no. of e⁻	core[a]	S	fragments	ref
54	**[FeFe₃S₄]²⁺**	2	Fe²⁺ (S = 0), [Fe₃S₄]⁰ (S = 2)	49
55	ᵖ[CoFe₃S₄]²⁺	¹/₂	Co²⁺ (S = ³/₂), [Fe₃S₄]⁰ (S = 2)	11, 25, c
56	ᵖ[CoFe₃S₄]¹⁺	(1)[d]	Co²⁺ (S = ³/₂), [Fe₃S₄]¹⁻ (S = ⁵/₂)	11, 25, c
	[NiFe₃S₄]²⁺ ᵇ	(1)[d]	Ni²⁺ (S = 1), [Fe₃S₄]⁰ (S = 2)	24, c
57	ᵖ[NiFe₃S₄]¹⁺	³/₂	Ni²⁺ (S = 1),]Fe₃S₄]¹⁻ (S = ⁵/₂)	15, 23, 24, c
58	ᵖ[MFe₃S₄]²⁺	2	M = Zn²⁺, Cd²⁺; [Fe₃S₄]⁰ (S = 2)	8, 13, e
59	ᵖ[MFe₃S₄]¹⁺	⁵/₂	M = Zn²⁺, Cd²⁺; [Fe₃S₄]¹⁻ (S = ⁵/₂)	8, 13

[a] Bold face, isolated cluster; p, protein-bound cluster. [b] Detected electrochemically. [c] This work. [d] Predicted spin and coupled fragments. [e] Surerus, K. K. Ph.D. Thesis, University of Minnesota, 1989.

enhance cluster stability, especially in the oxidized state. Given the relationship between solvent basicity and cluster stability,[41] it is apparent that large substituents tend to shield the electrophilic oxidized [Fe₄S₄]³⁺ core from solvent or other nucleophiles. Such substituents would be expected to play a similar role in heterometal cubane-type clusters.

¹H NMR Spectra. The spectra of clusters **6**, **7**, and **12**, presented in Figure 3, evidence substantial isotropic components to their chemical shifts with, for the most part, correspondingly well resolved features. Clusters with the [Fe₄S₄]²⁺ core such as **6** exhibit small isotropic shifts owing to population of paramagnetic states above the S = 0 ground state.[42] Clusters with the [CoFe₃S₄]²⁺ (**7, 8**)[25] and [NiFe₃S₄]¹⁺ (**9–12**)[23,24] cores have S = ¹/₂ and ³/₂ ground states, respectively (vide infra). The spectra have two conspicuous features. First, elementary considerations based on the signs of the isotropic shifts, which are set out in Table VI, indicate that the shifts are predominantly contact in origin. Contact interactions require that o-Me, m-H, and p-Me shifts of the mesitylthiolate ligand have the *same* sign,[43] as observed. Second, isotropic shifts at iron and cobalt or nickel subsites have the *opposite* sign. We have interpreted both of these features for [NiFe₃S₄]¹⁺ clusters[24] based on a simplified fragment formulation of [MFe₃S₄]²⁺ cores which is described in Table VII. Briefly, in this model the local spin of the M atom and the net spin of the Fe₃S₄ fragment are antiparallel coupled to give the system spin. The larger of the coupled spins is aligned parallel to the magnetic field, effecting ligand → metal antiparallel spin transfer and the induction of positive (α) spin into ligand donor atom orbitals which is then delocalized in a manner consistent with contact interactions.

Figure 6. ¹H NMR spectra of the reaction of [CoFe₃S₄(Smes)₄]²⁻ with 1 and 2 equiv of p-O₂NC₆H₄SH in CD₃CN solution at 297 K. The numbered signals refer to n = 0, 1, 2 in the product cluster formula [CoFe₃S₄(Smes)₄₋ₙ(SC₆H₄-p-NO₂)ₙ]²⁻. Spectra on the left and right refer to substituents at the iron and cobalt subsites, respectively. The features at 9.51 and 9.78 ppm are m-H signals of coordinated p-O₂NC₆H₄S⁻; all other signals are due to mesitylthiolate ligands.

The situation is reversed at the cobalt and nickel subsites; negative (β) spin is placed on donor atoms and delocalization results in oppositely signed shifts. In the absence of spin coupling, substituents on tetrahedral Ni(II) and Co(II) complexes exhibit shifts opposite to those in Table VI, as shown previously for Ni(II).[24] The isotropic shifts of tetrahedral [Co(Smes)₄]²⁻[44] in acetonitrile solution, −22.6 (m-H), −34.8 (o-Me), and −41.4 ppm (p-Me), are indicative of significant contact interactions and a reverse pattern of spin density distribution compared to **7**. As will be seen next, the spectral resolution usually afforded by isotropic shifts has proven indispensable in examining reactivity at different subsites.

Reactivity. (a) **Ligand Substitution.** The experiments described below were carried out in order to examine relative reactivities of metal subsites. They involve ca. 20 mM solutions of the indicated clusters in acetonitrile or Me₂SO solutions at ambient temperature. Because an extensive substitution chemistry of cluster **11** regiospecific to the nickel subsite has been described,[24] a similar study of **12** has not been carried out. However, this cluster has been examined in other potential ligand substitution systems. The reactions **6** in acetonitrile do not proceed to a detectable extent for at least 2 days, from which we infer that subsite affinity for Ph₃P falls in the order Ni > Fe, Co. Reaction 7 and the reaction of **12** with 3 equiv of NaSEt in Me₂SO affords the NiFe₃S₄ cluster mixture n = 1–3 as evidenced by resolved mesityl m-H and p-Me, phosphine m-H, and Fe–SCH₂ resonances (not shown).[45] Any cluster with the Ni–SEt subsite could not be detected. The clear implication from these reactions is that thiolate has a much more pronounced affinity for an iron than a nickel subsite, a matter further emphasized by the necessity to displace an anionic ligand upon substitution at the former subsite.

$$[NiFe_3S_4(PPh_3)(Smes)_3]^{2-} + [MFe_3S_4(Smes)_4]^{2-} \rightarrow N.R. \quad (6)$$
$$(M = Fe, Co)$$

$$[NiFe_3S_4(PPh_3)(Smes)_3]^{2-} + [Fe_4S_4(SEt)_4]^{2-} \rightarrow$$
$$[NiFe_3S_4(PPh_3)(Smes)_{3-n}(SEt)_n]^{2-} +$$
$$[Fe_4S_4(SEt)_{4-n}(Smes)_n]^{2-} \quad (7)$$

(41) (a) Blonk, H. L.; Kievit, O.; Roth, E. K.-H.; Jordanov, J.; van der Linden, J. G. M.; Steggerda, J. J. *Inorg. Chem.* **1991**, *30*, 3231. (b) Ohno, R.; Ueyama, N.; Nakamura, A. *Chem. Lett.* **1989**, 399.

(42) Reynolds, J. G.; Laskowski, E. J.; Holm, R. H. *J. Am. Chem. Soc.* **1978**, *100*, 5315.

(43) From the McConnell equation $a_i = Q\rho_{Ci}$, with Q_{CH} negative and Q_{CMe} positive, spin delocalization into the odd-alternate phenyl ring leads to C–H and C–CH₃ isotropic shifts of the same sign. Cf.: La Mar, G. N. In *NMR of Paramagnetic Molecules*; La Mar, G. N., Horrocks, W. D., Holm, R. H., Eds.; Academic Press: New York, 1973; Chapter 3.
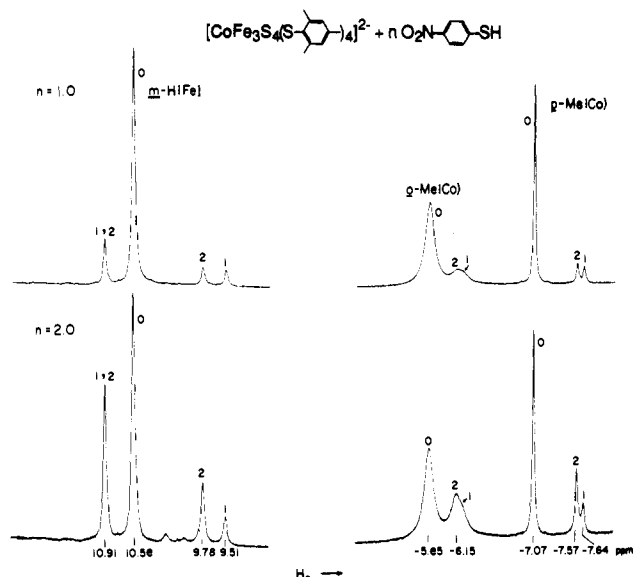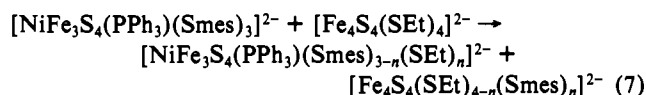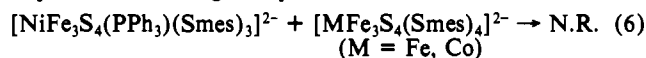
(44) This complex was prepared by the reaction of [CoCl₄]²⁻ with 4 equiv of NaSmes in acetonitrile and was isolated as its green Et₄N⁺ salt.

(45) Note that in reaction 7 and elsewhere, mixed-ligand Fe₄S₄ clusters (n = 1–3) are indicated as products. As shown by the reaction of **5** with 1–4 equiv of mesitylthiol in acetonitrile solution, the product clusters have essentially identical mesityl and ethyl chemical shifts even at 500 MHz. This unusual situation prevented detection of the separate mixed-ligand clusters.
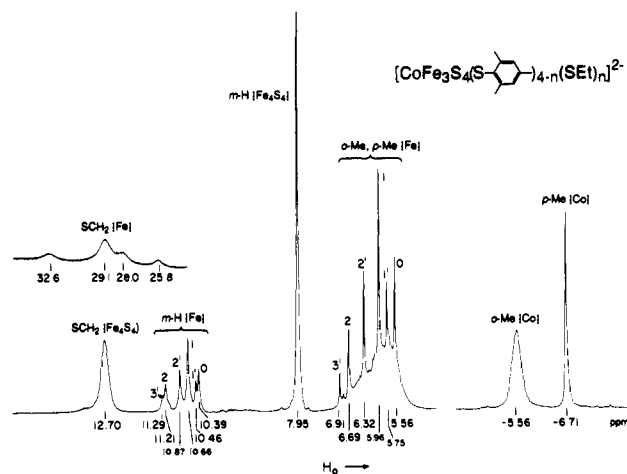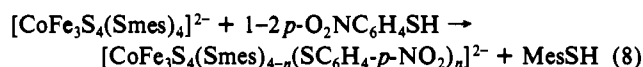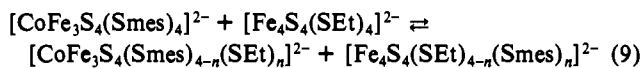
10850 *J. Am. Chem. Soc., Vol. 114, No. 27, 1992*

Zhou et al.

Figure 7. ^1H NMR spectra of the products of the reaction between equimolar $[CoFe_3S_4(Smes)_4]^{2-}$ and $[Fe_4S_4(SEt)_4]^{2-}$ in Me_2SO-d_6 solution at 297 K. The numbered signals $n = 0, 1, 2$ refer to species with the CoSmes group and $n = 1', 2', 3'$ to those with the CoSEt group in the set of clusters $[CoFe_3S_4(Smes)_{4-n}(SEt)_n]^{2-}$. Ligand subsites are indicated; Fe_4S_4 signals arise from $[Fe_4S_4(SEt)_{4-n}(Smes)_n]^{2-}$ whose separate cluster signals are not resolved. The 5.0 to -4.0 ppm spectral region, which is uninformative, is not shown.

Cluster **7** provides the unique opportunity to examine reactivity at iron and cobalt subsites with identical terminal ligands. In reaction 8, **7** in acetonitrile was treated with 1 and 2 equiv of

$$[CoFe_3S_4(Smes)_4]^{2-} + 1-2\,p\text{-}O_2NC_6H_4SH \rightarrow$$

$$[CoFe_3S_4(Smes)_{4-n}(SC_6H_4\text{-}p\text{-}NO_2)_n]^{2-} + MesSH \quad (8)$$

p-nitrobenzenethiol which, because it is much more acidic than mesitylthiol, effects stoichiometric ligand substitution. As shown in Figure 6, the $n = 1$ and 2 clusters are readily detected and identified from resonances of substituents at both the iron and cobalt subsites. Even though in the formation of the $n = 1$ and 2 clusters probability factors of 3 and 2, respectively, favor substitution at the iron subsites if all subsites are considered equivalent, any substitution at the cobalt site would have been readily detected. In fact, intensities of the Co–subsite resonances remained exactly constant when compared to Et_4N^+ resonances as an internal standard. Those of the Fe–subsite resonances were altered consistent with the formation of the indicated mixed-ligand clusters. Attempts to generate the $n = 3$ cluster, for which substitution probabilities are equal, were thwarted by slow decomposition of the $CoFe_3S_4$ species. We conclude that thiolate ligands at the iron subsites are more reactive to (thiolate) ligand substitution which proceeds by proton transfer to coordinated thiolate followed by coordination of the conjugate base of the proton donor.[46]

We have, however, observed ligand substitution at the cobalt subsite. Ligand redistribution occurs in systems containing clusters **5** and **7**, as represented by reaction 9. If substitution occurs at both the cobalt and iron subsites, some seven $CoFe_3S_4$ products

$$[CoFe_3S_4(Smes)_4]^{2-} + [Fe_4S_4(SEt)_4]^{2-} \rightleftharpoons$$

$$[CoFe_3S_4(Smes)_{4-n}(SEt)_n]^{2-} + [Fe_4S_4(SEt)_{4-n}(Smes)_n]^{2-} \quad (9)$$

are possible: those with the CoSmes group and $n = 1-3$ (signals 1–3), and those with the CoSEt group and $n = 1-4$ (signals 1'–4'). Reaction systems based on the initial mole ratios **5**:**7** $= 0.5$–2.0 in Me_2SO solutions were examined. The ^1H NMR spectrum of the equimolar reaction system is presented in Figure 7. The upfield set of signals arises from the CoSmes group, whose chemical shifts are evidently not sensitive to substitution at the iron subsites. Compared to the spectrum of pure **7**, these signals are slightly asymmetric and shifted but are unresolved. However, p-Me and o-H signals of mesitylthiolate ligands at iron subsites are well resolved and demonstrate the formation of at least five clusters. The former are superimposed on an envelope of broad

Table VIII. Electron Transfer Series of Heterometal Cubane Clusters

cluster	series/potentials[a]		ref
$[Fe_4S_4]^{3+} \rightleftharpoons [Fe_4S_4]^{2+} \rightleftharpoons [Fe_4S_4]^{1+}$ (10)			
$[Fe_4S_4(SEt)_4]^{2-}$	b	-1.29	24
$[Fe_4S_4(Smes)_4]^{2-}$	0.00	-1.20	c
$[Fe_4S_4(LS_3)(t\text{-}BuNC)_3]^{1-}$	-0.18	-1.08	49
$[CoFe_3S_4]^{3+} \rightleftharpoons [CoFe_3S_4]^{2+} \rightleftharpoons [CoFe_3S_4]^{1+}$ (11)			
$[CoFe_3S_4(Smes)_4]^{2-}$	-0.03	-1.02	c
$[CoFe_3S_4(Stib)_4]^{2-}$	d	-1.09	25
$[NiFe_3S_4]^{2+} \rightleftharpoons [NiFe_3S_4]^{1+} \rightleftharpoons [NiFe_3S_4]^0$ (12)			
$[NiFe_3S_4(SEt)_4]^{3-}$	-0.96	b	24
$[NiFe_3S_4(Smes)_4]^{3-}$	-0.90	b	c
$[NiFe_3S_4(PPh_3)(SEt)_3]^{2-}$	$-0.58^{b,e}$	-1.62	24
$[NiFe_3S_4(PPh_3)(Smes)_3]^{2-}$	$-0.50^{b,e}$	-1.55	c

^{a}V vs SCE in acetonitrile. ^{b}Irreversible. ^{c}This work. ^{d}Not reported. $^e E_{pa}$.

o-Me resonances. Signal assignments are based on changes in relative intensities as dependent on initial cluster mole ratios and on the assumption that substitution at an iron subsite will have a larger effect on the shifts of the remaining iron ligands than will substitution at the cobalt subsite.[47] Clusters with signals 3 and 4' would be very difficult to detect for they contain EtS^- ligands at all iron subsites. While multiple Fe–SCH_2 resonances with large downfield shifts are observed (Figure 7), their line widths and incomplete resolution do not permit assignments to specific clusters. These results confirm the expectation that iron and cobalt subsites in the same cluster are subject to facile substitution with a stronger ligand. While resonances cannot be accurately integrated because of partial overlap, the relative heights of signals 1 and 1' suggest that the first substitution reaction occurs primarily at an iron subsite, as favored by probability considerations. Lastly, detection of mixed-ligand clusters provides a further illustration of the sensitivity of isotropically shifted resonances to cluster substitution patterns.[48] Note the superior resolution of signals of mixed-ligand $[CoFe_3S_4]^{2+}$ vs $[Fe_4S_4]^{2+}$ clusters, a matter largely attributable to the ca. 3-fold larger isotropic shifts of the former (Table VI).

(b) Oxidation–Reduction. The cyclic voltammograms for **6**, **7**, and **12** indicate the presence of three oxidation levels of each cluster. As reported by Ueyama et al.,[28a] **6**, having bulky ligands, supports a well-defined oxidation. We also find a reversible reduction step, in contrast to the irreversible behavior described in DMF solution. Coulometry revealed $n = 1.0$ e^- for both steps. Similarly, the reduction of **7** gave $n = 1.0$ e^-. The oxidation of **7** and both redox steps of **12** produced species that suffered partial decomposition within the coulometric time scale (15 min for complete reaction of **4**). Despite the instability of these species, the results justify formulation of the three-member electron transfer series 10–12, presented in terms of core oxidation states in Table VIII. Potentials for members of each series follow the expected substituent effects. While we cannot interpret the origin of the behavior, introduction of a heterometal substantially influences the potential at parity of terminal ligand and cluster charge. Thus the potentials for the $[MFe_3S_4(Smes)_4]^{2-/3-}$ couples fall in the order M = Fe < Co < Ni, with potential differences relative to M = Fe being 0.18 V (Co) and 0.30 V (Ni). In the pair **5**/**9**, the potential difference is 0.35 V (Ni). The exception to this behavior is found with the oxidation of **6**/**7**, whose potentials differ by only 30 mV.

Table VIII contains all isolated or otherwise detected core oxidation states of $[MFe_3S_4]^{z+}$ of clusters with M = Co and Ni.

(46) Dukes, G. R.; Holm, R. H. *J. Am. Chem. Soc.* **1975**, *97*, 528.

(47) For example, resonances 1 (5.96, 10.66 ppm) and 1' (5.75, 10.46) were assigned to $n = 1$ clusters with CoSmes and CoSEt groups, respectively, because the latter are more nearly similar to the corresponding resonances of initial cluster **7** (5.56, 10.39 ppm). While the assignments in Figure 7 cannot be proven, they are consistent in corresponding to intuitive monotonic (downfield) p-Me and m-H shifts as the number of FeSEt groups increases.

(48) For related examples cf.: Palermo, R. E.; Holm, R. H. *J. Am. Chem. Soc.* **1983**, *105*, 4310 and references therein.
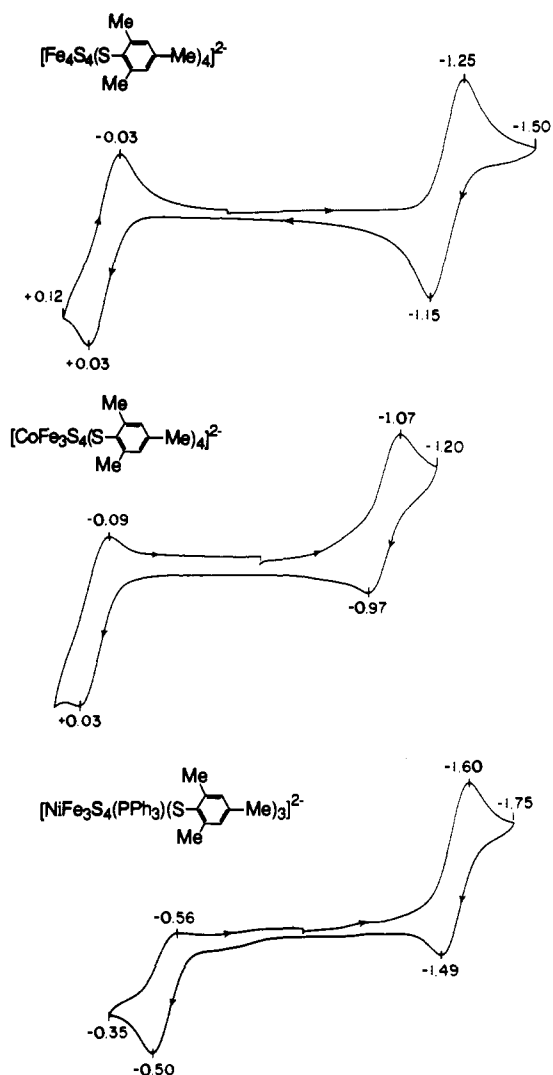
Figure 8. Cyclic voltammograms of [Fe₄S₄(Smes)₄]²⁻, [CoFe₃S₄-(Smes)₄]²⁻, and [NiFe₃S₄(PPh₃)(Smes)₃]²⁻ in acetonitrile solutions at 50 mV/s; peak potentials vs SCE are indicated.

Also included is [Fe₄S₄(LS₃)(*t*-BuNC)₃]¹⁻, a pseudoheterometallic species whose differentiated subsite contains six-coordinate low-spin Fe²⁺ in a cluster with spin $S = 2$.[49] Here the fragment formulation for a 54 e⁻ cluster (Table VII) has been shown to be meaningful by demonstration of the presence of a spin-isolated [Fe₃S₄]⁰ fragment. It would appear that the reversible redox steps of this cluster are best interpreted in terms of redox changes of the Fe₃S₄ fragment, as must be the case with the [MFe₃S₄]²⁺/¹⁺ redox steps of protein-bound zinc and cadmium clusters.[8] In series 11 and 12, the [MFe₃S₄]²⁺/¹⁺ couples presumably maintain the M²⁺ oxidation state, given the strongly reducing conditions and π-acid ligands normally required to stabilize tetrahedral Co¹⁺ and Ni¹⁺. The 3+/2+ couple of series 11 and the 1+/0 couple of series 12 may involve changes in the M atom oxidation state but, given the instabilities of the redox products, this point will be difficult to investigate. We next turn to the matter of electronic structures of clusters 7 and 12.

Electronic Structures. (a) [CoFe₃S₄(Smes)₄]²⁻. The EPR spectrum of cluster 7 in acetonitrile solution at ca. 10 K (not shown) is very similar to the published spectrum assigned to 8,[25] and corresponds to an $S = {}^1/_2$ ground state. The Mössbauer spectra of polycrystalline (Et₄N)₂[7] are presented in Figure 9. The zero field spectrum recorded at 4.2 K consists of one, albeit broadened, quadrupole doublet. The absence of magnetic hyperfine interactions is the result of spin–spin interactions which
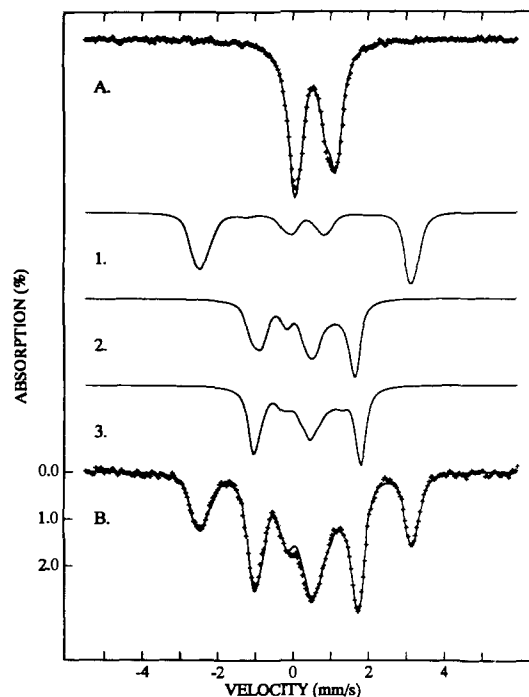
(49) Weigel, J. A.; Srivastava, K. K. P.; Day, E. P.; Münck, E.; Holm, R. H. *J. Am. Chem. Soc.* **1990,** *112,* 8015.

Figure 9. Mössbauer spectra of polycrystalline (Et₄N)₂[CoFe₃S₄(Smes)₄] recorded in zero applied magnetic field (A) and in a parallel field of 6.0 T at 1.5 K (B). The solid lines drawn through the spectra are simulations based on the $S = {}^1/_2$ spin Hamiltonian, eq 13. Curves 1, 2, and 3 are the theoretical spectra of the individual sites.

produce a near-zero time-averaged magnetic hyperfine field at the ⁵⁷Fe nucleus. In contrast to the magnetically dilute [CoFe₃S₄]²⁺ cluster in *Dg* Fd II/Co,[11] which yields resolved magnetic hyperfine interactions even in weak (<0.01 T) fields, strong applied fields are required to elicit resolved magnetic patterns for a polycrystalline sample of 7. A 6.0 T spectrum at 1.5 K is shown in Figure 9B. It has been analyzed with the $S = {}^1/_2$ spin Hamiltonian, eq 13, where A_i is the magnetic hyperfine tensor of site i, $H_Q(i)$ is the quadrupolar interaction, and the other symbols have their usual meanings. The sum is over iron sites $i = 1-3$.

$$H = 2\beta S \cdot H + \sum_{i=1}^{3} \{S \cdot A_i \cdot I_i - g_n\beta_n H \cdot I_i + H_Q(i)\} \qquad (13)$$

The spectrum of Figure 9B consists essentially of two subspectra with a 2:1 intensity ratio. The spectrum of site 3 has a magnetic hyperfine tensor with positive components whereas those of the other two sites are negative. Detailed spectral simulations suggest that sites 1 and 2 are slightly inequivalent. In contrast to the case of clusters 11 and 12 (vide infra), 7 has an isotropic electronic system. Therefore, the hyperfine parameters of the three sites are spatially uncorrelated, i.e., the coordinate x may refer to different directions for the three sites. The solid lines in Figure 9 are simulations of the spectra of individual sites based on eq 13 using the parameters in Table IX. Also given are the Mössbauer parameters of the [CoFe₃S₄]²⁺ cluster of *Dg* Fd II/Co. Clearly, the isomer shifts and magnetic hyperfine parameters (A_i) are essentially the same for the synthetic and protein-bound clusters.

(b) [NiFe₃S₄(PPh₃)(Smes)₃]²⁻. (i) Magnetism. The magnetic susceptibility of polycrystalline (Et₄N)₂[12] followed the Curie–Weiss law $\chi^M = C/(T - \theta)$ at 4.2–30 K with $C = 1.834$ emu/G and $\theta = -1.24$ K. The Curie constant demonstrates the $S = {}^3/_2$ ground state, for which the theoretical value is 1.875 emu/G with $g = 2$. As expected, cluster 12 has the same spin, and also similar isomer shift (δ), quadrupole splitting (Δ*E*Q), and *g* values, as 11.[24] However, our investigation of the electronic properties of 12 is much more complete than that of 11.

(ii) EPR Spectra. The X-band EPR spectra of (Et₄N)₂[12] in polycrystalline form and in frozen DMF and acetonitrile so-

Table IX. Mössbauer Spectroscopic Parameters of Synthetic and Protein-Bound MFe₃S₄ Clusters (M = Fe, Co, Ni) at 1.5 K

cluster/site	mm/s			MHz		
	δ^a	ΔE_Q	η^b	A_x	A_y	A_z
[Fe₄S₄(Smes)₄]²⁻ ᶜ	0.46	1.23				
[CoFe₃S₄(Smes)₄]²⁻						
site 1	0.45	1.04	0.4	−31.0 (8)	−37.0 (8)	−29.5 (5)
site 2	0.45	1.04	0.8	−37.3 (8)	−35.7 (8)	−31.8 (5)
site 3	0.38	−0.66	1.3	+29.8 (5)	+32.3 (5)	+29.8 (5)
Dg Fd II/Co*ᵈ*						
site 1,2	0.44	1.35	0.4	−35	−38	−32
site 3	0.35	−1.1	0.4	+27	+27	+32
[NiFe₃S₄(PPh₃)(Smes)₃]²⁻						
site 1ᵉ	0.48	−0.6		−8 (3)	−23 (3)	−(4−18)
site 2ᵉ	0.48	−1.1		−20 (4)	−23 (4)	−(14−33)
site 3ᵉ	0.48	−0.82		+19 (1)	+19 (1)	+4 (3)

ᵃ Relative to Fe metal at room temperature. ᵇ $\eta = (V_{xx} - V_{yy})/V_{zz}$. ᶜ 4.2 K. ᵈ Reference 11. ᵉ For A_x and A_y values the numbers in parentheses give the estimated uncertainties in the last significant figure; for A_z of sites 1 and 2, the ranges of compatible A_z values are given.
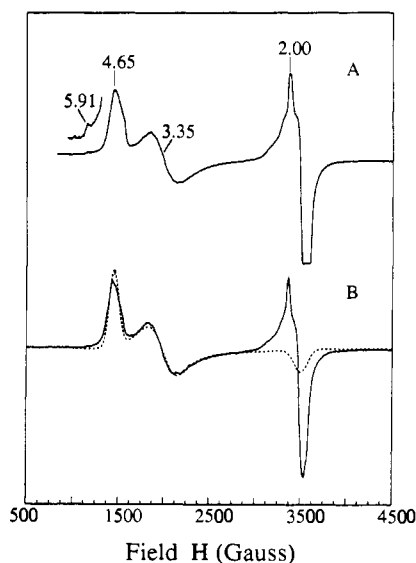

Field H (Gauss)

Figure 10. X-band EPR spectra of [NiFe₃S₄(PPh₃)(Smes)₃]²⁻ in DMF solution recorded at 16 K (A) and 4.2 K (B). The features at g_y = 4.65 and g_x = 3.35 belong to the $M_S = \pm^1/_2$ ground Kramers doublet of an $S = ^3/_2$ system; the corresponding resonance at g_z = 1.93 is partially masked by an unidentified radical signal at $g \approx 2$. The resonance at g_z = 5.91 (shown 6 times enlarged) is absent in part B because it derives from the $M_S = \pm^3/_2$ excited doublet. The dashed line in part B is a spectral simulation based on the $S = ^3/_2$ spin Hamiltonian, eq 13. In frozen acetonitrile solution, the same, but broader, signals are observed; this sample lacks the radical signal, unmasking the g_z = 1.93 ground state resonance.

lutions have been studied. While the observed resonances have the same *g* values in the two solutions, the better resolved spectra were obtained in DMF. Spectra at 16 K (A) and 4.2 K (B) are set out in Figure 10. The observed resonances are typical of those for an $S = ^3/_2$ system described by the spin Hamiltonian, eq 14, where *S* is the cluster spin, *D* and *E* are zero field splitting parameters, **g** is the **g** tensor, and the other symbols have their usual meanings. In zero magnetic field, the spin quartet is split into

$$H_e = D\left[\hat{S}_x^2 - \frac{5}{4} - \frac{E}{D}(\hat{S}_x^2 + \hat{S}_y^2)\right] = \beta \mathbf{S}\cdot\mathbf{g}\cdot\mathbf{H} \qquad (14)$$

two doublets separated by $\Delta = 2D[1 + 3(E/D)^2]^{1/2}$. Plots of the energy level diagram and *g* values for an $S = ^3/_2$ system are shown in Figure 11. For $|D| \gg \beta H$, it is common to assign each doublet a fictitious spin $S' = ^1/_2$ and an effective **g** tensor **g'**.

In the spectra of Figure 10, the region around *g* = 2 is masked by a contaminating radical species; the spin concentration of these unknown species is less than 20% of that giving rise to the $S = ^3/_2$ signals. (In acetonitrile, the radical species is absent, and a resonance at g_z' = 1.93 is observed.) The resonances at $g_y' \approx$ 4.65 and $g_x' \approx$ 3.35 belong to the $M_S = \pm^1/_2$ Kramers doublet; for E/D
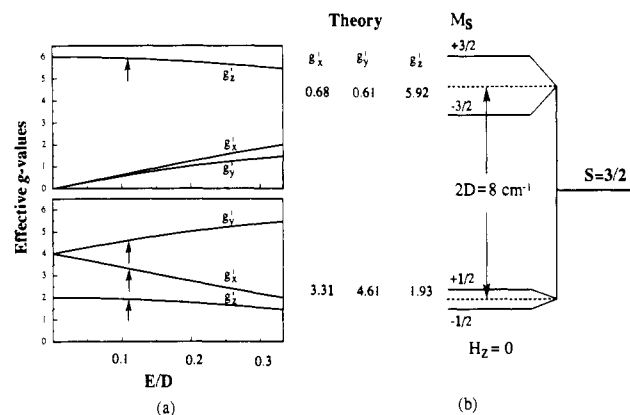

Figure 11. Effective *g* values of the two Kramers doublets (a) and energy level diagram of an $S = ^3/_2$ system computed from eq 14. The effective *g* values of (a) were computed by assuming that $g_x = g_y = g_z$ = 2.00. For E/D = 0.11, eq 14 predicts the effective *g* values in (b). Arrows in (a) identify the resonances observed for **12**. By choosing g_x = 2.03 and g_y = 2.01 in eq 14, the theoretical *g'* values match the experimental data.

= 0.11, eq 14 predicts g_y' = 4.63 and g_x' = 3.36 (Figure 11). The dashed curve in Figure 10B is a theoretical spectrum based on eq 14 for E/D = 0.11 and *g* = 2.03, 2.01, 2.00. In order to account for the width of the absorption lines, we have assumed that the parameter E/D has a gaussian distribution, with $\sigma(E/D)$ = 0.03. At 16 K, the EPR spectrum exhibits a weak resonance at g_z' = 5.91; this feature is absent at 4.2 K. This resonance belongs to the $M_S = \pm^3/_2$ Kramers doublet, for which eq 14 predicts for E/D = 0.11 an effective *g* value at g_z' = 5.92 for g_z = 2. The *g* = 5.91 feature is very weak, primarily because the intrinsic transition probability of this resonance, according to expressions given by Aasa and Vänngård,[50] is 55 times smaller than that of the *g* = 4.65 resonance. The temperature dependence of the spectrum shows that *D* > 0.

(iii) **Mössbauer Spectra.** Because of fast spin–spin relaxation, the Mössbauer spectra of polycrystalline (Et₄N)₂[**12**] measured in zero magnetic field consists of quadrupole doublets. A representative spectrum, recorded at 150 K, is shown in Figure 12A. The spectrum consists of a symmetric doublet showing that the three iron sites of the cluster are indistinguishable. We have improved the resolution of the spectra by using a Fourier deconvolution technique (which effectively removes the line width contribution of the source).

Cluster **12** has been studied in applied magnetic fields of 3.0, 5.0, 6.5, and 8.0 T at 4.2 and 1.5 K. A representative spectrum is shown in Figure 12B. We have analyzed the spectra in the framework of the $S = ^3/_2$ spin Hamiltonian, eq 14, augmented by the terms in eq 15 describing the hyperfine interactions with the ⁵⁷Fe nucleus. Given the number of unknowns, fitting of the Mössbauer spectra is a formidable task. For this reason and for
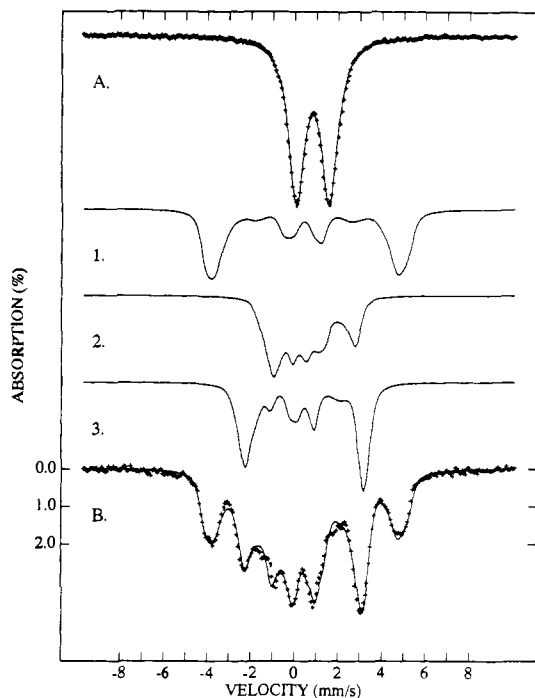
(50) Aasa, R.; Vänngård, T. *J. Magn. Reson.* **1975**, *19*, 308.

Synthesis of [MFe₃S₄]²⁺ Cubane-Type Clusters

J. Am. Chem. Soc., Vol. 114, No. 27, 1992 10853

Figure 12. Mössbauer spectra of polycrystalline $(Et_4N)_2[NiFe_3S_4$-$(PPh_3)(Smes)_3]$ recorded at 150 K in zero applied magnetic field (A) and in a parallel field of 8.0 T (B). The solid lines drawn through the spectra are simulations based on the $S = {}^3/_2$ spin Hamiltonian, eq 14. Curves 1, 2, and 3 show the contributions of the individual iron sites. The magnetic hyperfine tensor components $(A_x, A_y, A_z,$ in MHz) used here are the following: site 1, $-6.6, -23.8, -15.9$; site 2, $-18.5, -23.5, -20.7$; site 3, $+19.2, +18.9, +4.6$.

lack of optimal resolution, we have assumed that all tensors of eq 14 are collinear. By following the spectral patterns as a function

$$H = H_e + H_N \qquad (15)$$

$$H_N = \sum_{i=1}^{3} \{S \cdot A_i \cdot I_i - g_n\beta_n H \cdot I_i + H_Q(i)\}$$

$$\text{with } H_Q = \frac{eQV_{zz}(i)}{12}\left[3I_z^2(i) - \frac{15}{4} + \eta(i)(I_x^2(i) - I_y^2(i))\right]$$

of the applied magnetic field, three *magnetically inequivalent* sites can be discerned. The components of the magnetic hyperfine tensor of site 3 were found to be positive whereas those of sites 1 and 2 are negative. Because the iron sites are tetrahedral and therefore high-spin, the A tensor is dominated by the negative contributions of the Fermi contact term. Thus, a positive A tensor for site 3 implies that the local spin of that site is oriented antiparallel to the cluster spin S. The theoretical spectra for the cluster and the spectra of the subsites are shown in Figure 12. Some comments regarding the problem of determining the unknowns are in order.

For the spectral simulations, we fixed $E/D = 0.11$, as suggested by the EPR spectra. The parameter D was difficult to determine with precision because spin–spin relaxation problems in applied fields of less than 3.0 T restricted our analysis to the 1.5 K spectra obtained at fields greater than 3.0 T. Under these conditions, the internal magnetic field at the nucleus is almost saturated and the spectra are not very sensitive to D. However, we determined that $3 < D < 6$ cm^{-1}. For $E/D = 0.11$, the electronic system is essentially axial and for the ground level the expectation value of S_z is substantially smaller than those of S_x and S_y. Consequently, the powder-averaged Mössbauer spectrum is quite insensitive to the z components of the three magnetic hyperfine tensors. We stress that the spatial directions of the A tensors are correlated by reference to the anisotropic electronic system; i.e., x refers to the same direction for all sites. The spectrum of site 3 is best resolved and, therefore, its parameters are reasonably well determined. In order to fit the intensities of the outermost

magnetic lines for site 3, we had to reduce the value of A_z substantially relative to those of A_x and A_y. If A_z had a magnitude similar to A_x and A_y, the intensity pattern would imply that the recoilless fraction of site 3 is substantially smaller than those of sites 1 and 2. (This situation would be unprecedented for cubane-type clusters.) Not surprisingly, dependent on the magnitude and sign of ΔE_Q and the value of the asymmetry parameter η, we found that a substantial range of A_i values is compatible with the entire data set. Rather than quoting the specific parameters used to generate the spectra of sites 1–3 in Figure 12, we have listed in Table IX the range of A_i values for which suitable solutions could be found. The components of the electronic field gradient tensor correlate strongly with the A values, and the values for η are not reliable and are omitted from Table IX.

Electron Distributions and Fragment Formulations. For the clusters considered in this work, the cluster spin can be predicted by assuming that the ground multiplet is the state $|(S_{12},S_{34})S,M\rangle$, where $S_{12} = {}^9/_2$ is the spin of the delocalized pair of iron atoms and $S_{34} = S_3 + S_4$ results from parallel coupling of the spin of the third iron atom with the spin of M. Antiparallel coupling of S_{12} and S_{34} yields the cluster spin S. For $[CoFe_3S_4]^{2+}$ with $S_{12} = {}^9/_2$, $S_3 = {}^5/_2$, and $S_4(Co) = {}^3/_2$, the observed $S = {}^1/_2$ ground state is obtained. Similarly, for $[NiFe_3S_4]^{1+}$ with $S_{12} = {}^9/_2$, $S_3 = 2$, and $S_4(Ni) = 1$, the experimental value $S = {}^3/_2$ ensues.[51] For these clusters the same result is obtained by coupling Fe_3S_4 and M atom spins. This simplified description is used in the fragment formulations in Table VII. The oxidation state of M is inferred from the isomer shifts in Table IX and in series 16, which have been obtained from measurements on protein-bound $[Fe_3S_4]^{1+,0}$ and $[ZnFe_3S_4]^{1+}$ clusters.[1a,2,12,52,53] The mean isomer shift of **7** (0.42 mm/s) implies the formulation $Co^{2+} + [Fe_3S_4]^0$, which is used in the spin coupling model. The Fe_3S_4 fragment

$$[Fe_3S_4]^{1-} \qquad [Fe_3S_4]^0 \qquad [Fe_3S_4]^{1-} \qquad (16)$$
$$0.27 \ (Fe^{3+}) \ mm/s \quad 0.41-0.42 \ (Fe^{2.67+}) \ mm/s \quad 0.55-0.56 \ (Fe^{2.33+}) \ mm/s$$

of **12** appears to be somewhat more reduced than **6** or the fragment of **7** on the basis of isomer shifts and Fe–SR terminal bond distances. These data point to the fragment formulation $Ni^{2+} + [Fe_3S_4]^{1-}$, but with recognition that substantially more charge has been delocalized on the nickel site than on the zinc site in $[ZnFe_3S_4]^{1+}$. The spin coupling scheme described here is rudimentary. More examples of spin-coupled MFe_3S_4 clusters containing first transition series heteroatoms are needed to test the scheme. Certainly, more theoretical work aimed at understanding the magnetic hyperfine interactions with attention to the observed valence delocalization is required to elucidate the details of magnetic coupling.

Summary. The following are the principal results and conclusions of this investigation. Certain information from our previous study[23,24] is also noted.

(1) Preparative routes potentially or actually affording heterometal cubane-type clusters with $[MFe_3S_4]^{z+}$ cores have been outlined (Table V). Clusters containing the $[CoFe_3S_4]^{2+}$ (**7**) and $[NiFe_3S_4]^{1+}$ (**9–12**) cores can be prepared by reductive rearrangement reactions of linear trinuclear clusters (**3, 4**) with Co(I)

(51) These observations suggest that the coupling scheme is strongly influenced by double exchange within the delocalized Fe³⁺·Fe²⁺ pair which gives rise to parallel spin alignment and $S_{12} = {}^9/_2$.[13] If the interactions between S_3 and S_4 are antiferromagnetic with moderate coupling strength or are ferromagnetic, antiferromagnetic coupling of S_1 and S_2 with S_3 and S_4 would favor a ground state that is predominantly $|({}^9/_2,S_{34})S,M\rangle$. We have considered whether the g values obtained for **12** give any decisive clues to the coupling scheme. However, the closeness of the g values of the $S = {}^3/_2$ system (2.03, 2.01, 2.00) to $g = 2$, together with the lack of knowledge regarding the relative orientations of the local g tensors, does not allow us to narrow down the possible choices.

(52) (a) Emptage, M. H.; Kent, T. A.; Huynh, B. H.; Rawlings, J.; Orme-Johnson, W. H.; Münck, E. *J. Biol. Chem.* **1980**, *255*, 1793. (b) Huynh, B. H.; Moura, J. J. G.; Moura, I.; Kent, T. A.; LeGall, J.; Xavier, A. V.; Münck, E. *J. Biol. Chem.* **1980**, *255*, 3242.

(53) Srivastava, K. K. P.; Surerus, K. K.; Conover, R. C.; Johnson, M. K.; Park, J.-B.; Adams, M. W. W.; Münck, E. *Inorg. Chem.*, submitted for publication. A Mössbauer study of *Pf* Fd/Ni[15] has shown that, within the still substantial uncertainties, the parameters of the protein cluster are the same as those obtained here for **12**.

and Ni(0) precursors, respectively. Use of the bulky mesityl-thiolate ligand improves both yields and solution stabilities of the clusters. The reductive rearrangement approach should be capable of extension to other clusters.

(2) Cubane-type structures have been demonstrated by X-ray diffraction of compounds containing clusters 7–12; M and Fe subsites are tetrahedrally coordinated. In heterometal clusters with four identical terminal ligands, the M and Fe subsites are disordered. Core dimensions closely parallel those of the homo-metallic $[Fe_4S_4]^{2+}$ clusters.

(3) ^1H NMR spectra of $[CoFe_3S_4]^{2+}$ and $[NiFe_3S_4]^{1+}$ clusters are characterized by substantial or dominant contact contributions to the isotropic shifts, which are oppositely signed for substituents at the Fe and M = Co/Ni subsites owing to antiferromagnetic coupling between M and Fe_3S_4 cluster fragments. It is noteworthy that at room temperature the three iron sites are equivalent by NMR, but in the solid state at 4.2 K two of the sites have a negative, and one a positive, expectation value of the local spin (Table IX).

(4) In $[CoFe_3S_4]^{2+}$ (7), the Fe subsites appear more susceptible to thiolate ligand substitution proceeding by proton transfer from incoming thiolate, whereas both Co and Fe subsites are substituted when one thiolate ligand is replaced by another in the ligand redistribution system 5/7.

(5) The three-member electron transfer series $[CoFe_3S_4]^{3+/2+/1+}$ and $[NiFe_3S_4]^{2+/1+/0}$ have been established, similar in scope to the $[Fe_4S_4]^{3+/2+/1+}$ series of homometallic clusters. Introduction of a heterometal M = Co/Ni at parity of charge and terminal ligand in the series of reversible couples $[MFe_3S_4(Smes)_4]^{2-,3-}$ affords the potential order M = Fe < Co (0.18 V) < Ni (0.30 V), with the indicated potential differences vs M = Fe.

(6) The electronic structure of synthetic (7) and protein-bound $[CoFe_3S_4]^{2+}$ are equivalent, containing a delocalized $Fe^{3+}\cdot Fe^{2+}$ pair, an Fe^{3+} site, and a Co^{2+} site. Isomer shifts support the corresponding Co^{2+} ($S = 3/2$) + $[Fe_3S_4]^0$ ($S = 2$) fragment formulation, with antiparallel spin coupling affording an $S = 1/2$ ground state. In contrast, the synthetic $[NiFe_3S_4]^{1+}$ core (11, 12) contains three indistinguishable iron sites. Isomer shifts and structural data suggest the antiparallel coupled Ni^{2+} ($S = 1$) and

$[Fe_3S_4]^{1-}$ ($S = 5/2$) fragments with an $S = 3/2$ ground state.

(7) The near-identity of Mössbauer parameters for 7 and *Dg* Fd II/Co and for 12 and *Pf* Fd/Ni[53] and the close similarity of the EPR spectra of 11/12 and *Pf* Fd/Ni[15] provide persuasive evidence, in the absence of protein crystallographic results, that *the protein-bound clusters contain the heterometal tightly integrated into the MFe₃S₄ cores* in the manner demonstrated by X-ray diffraction of the synthetic clusters.

Lastly, we note the continually increasing number of examples of cuboidal Fe_3S_4 clusters 1 in proteins and enzymes and the probability that such clusters are not always degradation products of native Fe_4S_4 clusters.[54] Consequently, there exists the prospect that such clusters may engage in heterometal binding in vivo and that biological functions may emerge for protein-bound MFe_3S_4 clusters 2 or a fragment thereof, such as cuboidal MFe_3S_3. While one possible instance of a biological $NiFe_3S_4$ cluster, in the carbon monoxide dehydrogenase of *Rhodospirillum rubrum*, has been disproved,[55] the possible occurrence of heterometal clusters in biology should nonetheless be actively entertained.

Supplementary Material Available: Crystallographic data for the compounds in Table II, including tables of intensity collections, atom and thermal parameters, bond distances and angles, and calculated hydrogen atom positions (18 pages); listings of calculated and observed structure factors (57 pages). Ordering information is given on any current masthead page.

(54) For a recent discussion of this point, cf.: Knaff, D. B.; Hirasawa, M.; Ameyibor, E.; Fu, W.; Johnson, M. K. *J. Biol. Chem.* **1991,** *266,* 15080 and references therein.

(55) Tan, G. O.; Ensign, S. A.; Ciurli, S.; Scott, M. J.; Hedman, B.; Holm, R. H.; Ludden, P. W.; Korzun, Z. R.; Stephens, P. J.; Hodgson, K. O. *Proc. Natl. Acad. Sci. U.S.A.* **1992,** *89,* 4427.